Journal of Computational Mathematics
Vol.xx, No.x, 2025, 1–25.

http://www.global-sci.org/jcm
doi:10.4208/jcm.2504-m2024-0272

NEWTON ITERATIVE INVERSION METHOD FOR INVERSE OBSTACLE SCATTERING IN A LAYERED MEDIUM*

Hao Wu and Jiaqing Yang[1)]
School of Mathematics and Statistics, Xi'an Jiaotong University, Xi'an 710049, China
Emails: wuhao2022@stu.xjtu.edu.cn, jiaq.yang@mail.xjtu.edu.cn

Abstract

Consider the inverse acoustic scattering of time-harmonic point sources by a locally perturbed interface with bounded obstacles embedded in the lower half-space. A Newton-type iterative method is proposed to simultaneously reconstruct the locally rough interface and embedded obstacles by taking partial near-field measurements in the upper half-space. The method relies on a differentiability analysis of the scattering problem with respect to the locally rough interface and the embedded obstacle, which is established by introducing a kind of new shape derivatives and reducing the original model to an equivalent system of integral equations defined in a bounded domain. With a slight modification, the inversion method can be easily generalized to reconstruct local perturbations of a global rough interface. Finally, numerical results are presented to illustrate the effectiveness of the inversion method with the multi-frequency data.

Mathematics subject classification: 65N21, 78A46, 35J05.
Key words: Newton iterative algorithm, Shape derivative, Inverse scattering, Locally rough interface, Embedded obstacle, Multi-frequency data.

1. Introduction

This paper is concerned with the two-dimensional inverse scattering of time-harmonic acoustic point sources by a locally rough interface with bounded obstacles embedded in the lower half-space. Such problems can find important applications in diverse scientific fields such as geophysics, underwater exploration and nondestructive testing, where the unbounded interface and embedded obstacles need to be reconstructed simultaneously from scattered field measurements over certain subdomains of the upper half-space.

In this paper, we consider the interface to be different from the planar interface over a finite interval, namely, locally rough surfaces. In this case, the whole space is divided into the upper and lower half-space, where an impenetrable obstacle is assumed to be embedded in the lower half-space. Considering a point source as an incident wave, then the wave motion is governed by the two-dimensional Helmholtz equation with a piecewise constant wavenumber. Since the interface is locally perturbed, the classical Sommerfeld radiation condition can be used to guarantee the uniqueness of the solution to the scattering problem. In the above setting, it is well-known that if there are no embedded obstacles, the well-posedness has been proved in associated function spaces by either the variational method, e.g. [2, 7, 43], or the integral equation method, e.g. [9, 10, 25, 38]. For the case of the presence of embedded obstacles, it was shown in [45] that a new technique was proposed to prove the well-posedness by reducing

* Received November 27, 2024 / Revised version received March 11, 2025 / Accepted April 3, 2025 / Published online June 18, 2025 /
[1)] Corresponding author

the original problem into an integral equation defined on a bounded region. Motivated by this technique, we study in this paper the inverse problem for simultaneously recovering the infinite interface and embedded obstacles from the near-field measurements. It is noticed in [45] that a global uniqueness theorem has been proved that the interface and embedded obstacles can be uniquely determined from near-field measurements on a bounded line segment in the upper half-space. With this result, we aim to develop an efficient algorithm to solve the inverse problem numerically. Notice that if there are no embedded obstacles, many inversion algorithms are developed for solving inverse rough interface scattering problems in the literature such as the Kirsch-Kress method [26], Newton-type algorithms [11,42], algorithms based on the transformed-field expansions [4], and non-iterative qualitative methods [27, 30, 31, 36, 46]. For the case of a planar interface with buried obstacles, we refer to the MUSIC-type scheme [1], the asymptotic factorization method [15], the sampling method [14], and the direct imaging algorithm [24, 29]. More generally, for the case of a rough interface with buried obstacles, the inversion algorithm was recently proposed in [28], which proposes a new version of the linear sampling method (LSM) for the numerical recovery of rough interfaces and embedded obstacles by constructing a modified near-field equation. Compared to the non-iterative LSM method, which can provide a good initial value for the iterative method, we aim to develop a Newton-type iterative method to further accurately recover the shape of the interface and embedded obstacles. As related works, we also refer to [3, 5, 6, 8, 13, 22, 23, 33, 34, 41, 44, 47] for the case of impenetrable rough surfaces.

The iterative method is a popular approach to solve the inverse scattering problem, where the key point is to analyze the Fréchet differentiability of the far-field or near-field with respect to the scatterer or physical parameters. A lot of literature can be found on Fréchet differentiability analysis, but they are mostly restricted to the case of bounded obstacles, e.g. [17–21, 37, 39, 40]. It is more challenging for infinite surface scattering problems, especially for the penetrable interfaces case. So far, the relevant results can only be provided when the surface is impenetrable and locally rough. It was shown by Bao and Lin [5] that the Fréchet differentiability analysis of the inverse locally rough scattering problem with a Dirichlet boundary condition can be proved based on the Dirichlet reflection principle of the Laplace operator. This approach was also extended by Qu *et al.* [41] into the inverse locally rough scattering problems with a Neumann boundary condition. However, the reflection principle fails in the impedance and penetrable interface scattering problems. Recently, Liu and Yang [35] established the Fréchet differentiability analysis of locally rough surfaces with Dirichlet and impedance boundary by transforming the original problem into a bounded boundary integral equation and repeatedly using Green's theorem. Nevertheless, this approach also fails in the case of penetrable interfaces, because in this case the scattering problem cannot be transformed into a bounded boundary integral equation, and to the authors' knowledge, there is no related works on Fréchet differentiability analysis for infinite rough interface scattering problems.

In this paper, we will propose a Newton-type iterative method to simultaneously reconstruct the locally rough interface and embedded obstacles, in which the main difficulty is how to establish the corresponding Fréchet differentiability analysis. In order to overcome this difficulty, we will first introduce the concept of shape derivatives, where the shape transformation function are defined, which allows us to use the one-dimensional variables t and s to characterize the shape variation of rough interfaces and embedded obstacles. Further, we introduce the perturbation problem with respect to t and s. With the help of a special hemispherical interface problem, the perturbation problem can also be reduced to a system of integral equations de-

fined on a bounded region. We can then prove that the near-field is differentiable with respect to t and s at 0 by showing that the integral operators are differentiable, respectively. Finally, we give a characterization of the shape derivative of the near-field which is proved to be the solution of a certain forward scattering problem by using the potential theory. With this result, we propose a Newton-type iterative algorithm to numerically reconstruct the locally rough interface and embedded obstacles simultaneously. Numerical results show that the algorithm works well for the simultaneous reconstruction of infinite interfaces and buried obstacles even in high noise levels.

The rest of this paper is organized as follows. In Section 2, we introduce the mathematical formulation of the scattering problem and reduce it to a system of integral equations defined on bounded regions. In Section 3, we give shape derivatives of the scattered field with respect to the infinite interface and embedded obstacles, respectively, along with the characterization of derivatives. In Section 4, we propose a Newton-type algorithm with multi-frequency data to simultaneously recover the locally rough interface and embedded obstacles in the lower half-space. In Section 5, we give some numerical results to demonstrate the effectiveness of the algorithm. Finally, some conclusions are given in Section 6.

2. Mathematical Formulation

As in Fig. 2.1, the scattering interface is described as

$$\Gamma := \big\{(x_1, x_2) \in \mathbb{R}^2 : x_2 = f(x_1)\big\},$$

where f is a Lipschitz continuous function with compact support, which indicates that the scattering interface is a local perturbation of the planar interface. The scattering interface Γ divides $\mathbb{R}^2$ into two parts

$$\Omega_1 := \big\{(x_1, x_2) \in \mathbb{R}^2 : x_2 > f(x_1)\big\},$$
$$\Omega_2 := \big\{(x_1, x_2) \in \mathbb{R}^2 : x_2 < f(x_1)\big\},$$

where Ω_1 and Ω_2 denote the upper and lower half-spaces, respectively. Let the upper half-space equip with the wavenumber κ_1 and the lower half-space equip with the wavenumber κ_2. Moreover, we assume that D is a bounded and simply-connected obstacle embedded in the lower half-space and that $\partial D \in C^{2,\alpha}, 0 < \alpha \leq 1$.

Consider the point source

$$\Phi_{\kappa_1}(x, z) := \frac{i}{4} H_0^{(1)}(\kappa_1 |x - z|), \quad x \neq z, \quad z \in \Omega_1$$

as the incident field u^i, where $H_0^{(1)}(\cdot)$ is the Hankel function of the first kind of order zero and $\Phi_{\kappa_1}(\cdot\,,\cdot)$ is the fundamental solution of the Helmholtz equation in free space, i.e. $\Phi_{\kappa_1}(\cdot, z)$

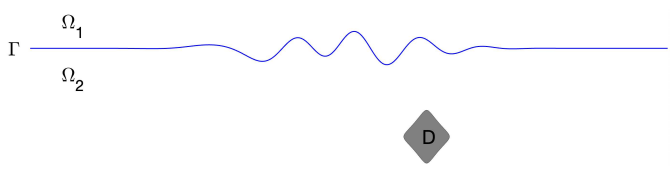

Fig. 2.1. The physical configuration of the scattering problem.

satisfies the equation

$$\Delta\Phi_{\kappa_1}(\cdot,z)+\kappa_1^2\Phi_{\kappa_1}(\cdot,z)=-\delta_z(\cdot)$$

in the distribution sense. Here, $\delta_z(\cdot):=\delta(\cdot-z)$ is the Kronecker delta distribution. Then the scattering of $u^i(\cdot,z)$ by Γ and D can be modeled by the two-dimensional Helmholtz equation

$$\Delta u+\kappa^2 u=-\delta_z \quad \text{in } \mathbb{R}^2\backslash\bar{D}, \tag{2.1}$$

where the wavenumber $\kappa>0$ is defined as the piecewise constant, i.e. $\kappa=\kappa_1$ in Ω_1 and $\kappa=\kappa_2$ in Ω_2, and u is the total field defined as $u:=u^i+u^s$ in Ω_1 and $u:=u^s$ in $\Omega_2\backslash\bar{D}$. For simplicity, we consider embedded obstacles to be sound-soft, i.e. u satisfies the Dirichlet boundary condition

$$u=0 \quad \text{on } \partial D. \tag{2.2}$$

Since Γ is a locally rough interface, we can suppose that the scattered field u^s satisfies the Sommerfeld radiation condition

$$\lim_{r\to\infty}\sqrt{r}\left(\frac{\partial u^s}{\partial r}-\mathrm{i}\kappa u^s\right)=0, \quad r=|x| \tag{2.3}$$

uniformly in all directions $\hat{x}:=x/|x|\in\mathbb{S}=\{x\in\mathbb{R}^2:|x|=1\}$. It is noted that the Sommerfeld radiation condition (2.3) can be replaced by the much weaker upward and downward propagating radiation conditions (cf. [10]) for the general rough interface case, which can be shown to be equivalent to (2.3) for the locally rough interface case. For a more detailed discussion the reader is referred to, e.g. [13, 26].

2.1. Special hemispheric interface problem

In this subsection, we introduce the special hemispheric interface problem. As shown in the Fig. 2.2, we introduce the special hemisphere interface

$$\Gamma_R:=\Big\{(x_1,x_2)\in\mathbb{R}^2 \,:\, x_2=0 \text{ for } |x_1|\geq R, \text{ and } x_2=\sqrt{R^2-x_1^2} \text{ for } |x_1|<R\Big\}.$$

Then, Γ_R divides $\mathbb{R}^2$ into two parts $\Omega_{1,R}$ and $\Omega_{2,R}$. Using the point source wave $\Phi_{\kappa_i}(x,z)$, $i=1,2$, as the incident field, we have

$$\begin{cases}\Delta G_R+\kappa_R^2 G_R=-\delta_z & \text{in } \mathbb{R}^2\backslash\{z\}\\ \lim\limits_{r\to\infty}\sqrt{r}\left(\dfrac{\partial G_R^{\mathrm{s}}}{\partial r}-\mathrm{i}\kappa_R G_R^{\mathrm{s}}\right)=0, & r=|x|,\end{cases} \tag{2.4}$$

where $\kappa_R=\kappa_1$ in $\Omega_{1,R}$ and $\kappa_R=\kappa_2$ in $\Omega_{2,R}$. It is clearly seen (cf. [45]) that

$$\begin{aligned}
&G_R(x,z)=G^s_{R,1}(x,z)+\Phi_{\kappa_1}(x,z), && x\in\Omega_{1,R}, && z\in\Omega_{1,R},\\
&G_R(x,z)=G^s_{R,2}(x,z), && x\in\Omega_{2,R}, && z\in\Omega_{1,R},\\
&G_R(x,z)=G^s_{R,3}(x,z), && x\in\Omega_{1,R}, && z\in\Omega_{2,R},\\
&G_R(x,z)=G^s_{R,4}(x,z)+\Phi_{\kappa_2}(x,z), && x\in\Omega_{2,R}, && z\in\Omega_{2,R},
\end{aligned}$$

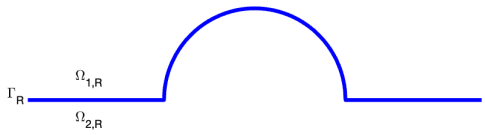

Fig. 2.2. Special hemispherical interface.

where $G^s_{R,1}(x,z)$ and $G^s_{R,4}(x,z)$ are scattered waves, and $G^s_{R,2}(x,z)$ and $G^s_{R,3}(x,z)$ are transmitted waves.

2.2. Perturbation problem

In this subsection, we introduce the shape transformation function and the perturbation problem for (2.1)-(2.3). Firstly, we give a few notations.

Definition 2.1. $\mathrm{Lip}(\mathbb{R}^2)$*: The set of bounded Lipschitz functions from* $\mathbb{R}^2$ *to* $\mathbb{R}^2$.

Definition 2.2. $C^\infty(\mathbb{R}^2)$*: The set of infinite order differentiable functions from* $\mathbb{R}^2$ *to* $\mathbb{R}^2$.

Definition 2.3. *Define the diffeomorphism* $\psi : t \in [0,T) \mapsto \psi(t,\cdot) \in \mathrm{Lip}(\mathbb{R}^2)$ *second order differentiable at* $t=0$ *with* $\psi(0,\cdot) = \boldsymbol{I}$, $\partial_t\psi(0,x) = \boldsymbol{V}(x) \in C^\infty(\mathbb{R}^2)$ *and* $\partial_t^2\psi(0,x) = \boldsymbol{U}(x) \in C^\infty(\mathbb{R}^2)$. *In particular, we assume* $\boldsymbol{V}(x) = 0$ *for any* $x \in \Gamma_R$.

Definition 2.4. *Define the diffeomorphism* $\phi : s \in [0,S) \mapsto \phi(s,\cdot) \in \mathrm{Lip}(\mathbb{R}^2)$ *second order differentiable at* $s=0$ *with* $\phi(0,\cdot) = \boldsymbol{I}$, $\partial_s\phi(0,x) = \mathscr{V}(x) \in C^\infty(\mathbb{R}^2)$ *and* $\partial_s^2\phi(0,x) = \mathscr{U}(x) \in C^\infty(\mathbb{R}^2)$.

For convenience, we denote

$$\Gamma_t := \psi(t,\Gamma), \quad x_t := \psi(t,x), \quad \partial D_s := \phi(s,\partial D), \quad x_s := \phi(s,x).$$

Meanwhile, we define the Jacobian determinants of $\psi(t,x)$ and $\phi(s,x)$ by $J(t,x)$ and $\mathscr{J}(s,x)$, respectively. From the above definition, it can be seen that $\psi(t,x)$ describes the deformation of Γ_t and $\phi(s,x)$ describes the deformation of ∂D_s.

With the above shape transformation functions ψ and ϕ, we introduce the perturbation problem

$$\begin{cases} \Delta u_{t,s} + \kappa_t^2 u_{t,s} = -\delta_z & \text{in } \mathbb{R}^2\backslash\bar{D}_s, \\ u_{t,s} = 0 & \text{on } \partial D_s, \\ \lim\limits_{r\to\infty} \sqrt{r}\left(\dfrac{\partial u^{\mathrm{s}}_{t,s}}{\partial r} - \mathrm{i}\kappa_t u^{\mathrm{s}}_{t,s}\right) = 0, & r = |x| \end{cases} \tag{2.5}$$

of (2.1)-(2.3), where the wavenumber $\kappa_t > 0$ is defined as the piecewise constant, i.e. $\kappa_t = \kappa_1$ in $\Omega_{t,1}$ and $\kappa_t = \kappa_2$ in $\Omega_{t,2}$. Here, $\Omega_{t,1}$ and $\Omega_{t,2}$ are the upper half-space and the lower half-space corresponding to Γ_t.

Note that $G_R(x,y)$ contains the information of Γ_R, and the solution $u_{t,s}$ of (2.5) contains the information of Γ_t. Naturally, we consider the difference $v_{t,s}(\cdot,z) := u_{t,s}(\cdot,z) - G_R(\cdot,z)$. Then, according to (2.4) and (2.5), $v_{t,s}$ satisfies the following problem:

$$\begin{cases} \Delta v_{t,s} + \kappa_R^2 v_{t,s} = g_{t,s} & \text{in } \mathbb{R}^2\backslash\bar{D}_s, \\ v_{t,s} = -G_R & \text{on } \partial D_s, \\ \lim\limits_{r\to\infty} \sqrt{r}\left(\dfrac{\partial v_{t,s}}{\partial r} - \mathrm{i}\kappa_R v_{t,s}\right) = 0, & r = |x|, \end{cases} \tag{2.6}$$

where $\eta := \kappa_2^2 - \kappa_1^2$, $B_t := \psi(t,B)$,

$$B := \Big\{(x_1,x_2) \in \mathbb{R}^2 \,:\, f(x_1) < x_2 < \sqrt{R^2 - x_1^2} \text{ for } |x_1| < R\Big\},$$

$$g_{t,s} := \begin{cases} \eta u_{t,s}(\cdot,z) & \text{in } B_t, \\ 0 & \text{in } \mathbb{R}^2\backslash\bar{B}_t. \end{cases}$$

We set R large enough to make the hemisphere fully contain the local perturbations. For the sake of convenience, we denote the boundary $\partial B := S_R^+ \cup \tilde{\Gamma}_R$ of the domain B, where

$$\tilde{\Gamma}_R := \{(x_1, x_2) \in \Gamma : |x_1| < R\},$$
$$S_R^+ := \Big\{(x_1, x_2) \in \mathbb{R}^2 \,:\, |x_1| < R \text{ and } x_2 = \sqrt{R^2 - x_1^2}\Big\}.$$

In order to demonstrate the existence of the solution of the scattering problem (2.5), we introduce the following potential operators with the kernel $G_R(x, y)$:

$$\begin{aligned}
T_t\psi(x) &:= \int_B G_R(x_t, y_t)|J(t, y)|\psi(y)\,\mathrm{d}y, && x \in B,\\
\tilde{T}_{t,s}\psi(x) &:= \int_B G_R(x_s, y_t)|J(t, y)|\psi(y)\,\mathrm{d}y, && x \in \partial D,\\
S_s\varphi(x) &:= 2\int_{\partial D} G_R(x_s, y_s)|\mathscr{J}(s, y)|\varphi(y)\,\mathrm{d}s(y), && x \in \partial D,\\
\tilde{S}_{t,s}\varphi(x) &:= \int_{\partial D} G_R(x_t, y_s)|\mathscr{J}(s, y)|\varphi(y)\,\mathrm{d}s(y), && x \in B,\\
K_s\varphi(x) &:= 2\int_{\partial D} \frac{\partial G_R(x_s, y_s)}{\partial \nu_s(y_s)}|\mathscr{J}(s, y)|\varphi(y)\,\mathrm{d}s(y), && x \in \partial D,\\
\tilde{K}_{t,s}\varphi(x) &:= \int_{\partial D} \frac{\partial G_R(x_t, y_s)}{\partial \nu_s(y_s)}|\mathscr{J}(s, y)|\varphi(y)\,\mathrm{d}s(y), && x \in B,
\end{aligned}$$

where $x_t = \psi(t, x), y_t = \psi(t, y), x_s = \phi(s, x), y_s = \phi(s, y)$, and ν_s denotes the exterior unit normal vector to ∂D_s.

Since $G_R(x, y)$ and $\Phi_{\kappa_i}(x, y)$ have the same singularity in the neighborhood of $x = y$, it follows from [12] that S_s and K_s are bounded and compact operators from $H^{1/2}(\partial D)$ into $H^{1/2}(\partial D)$, and T_t is a bounded and compact operator from $L^2(B)$ into $L^2(B)$, and $\tilde{S}_{t,s}$ and $\tilde{K}_{t,s}$ are bounded and compact operators from $H^{1/2}(\partial D)$ into $L^2(B)$, and $\tilde{T}_{t,s}$ is a bounded and compact operator from $L^2(B)$ into $H^{1/2}(\partial D)$.

For (2.6), we look for a solution to (2.5) in the form

$$\begin{aligned}
u_{t,s}(x, z) = G_R(x, z) &- \eta\int_B G_R(x, y_t)|J(t, y)|\,\tilde{u}_{t,s}|_B(y, z)\,\mathrm{d}y\\
&- \int_{\partial D}\left\{\frac{\partial G_R(x, y_s)}{\partial \nu(y)} - i\rho G_R(x, y_s)\right\}|\mathscr{J}(s, y)|\tilde{\varphi}_{t,s}(y, z)\,\mathrm{d}s(y)
\end{aligned} \tag{2.7}$$

for $x \in \mathbb{R}^2\backslash\{\partial\bar{D}_s \cup z\}$ with density functions

$$\tilde{u}_{t,s}|_B(\cdot, z) := u_{t,s}|_{B_t}\big(\psi(t, \cdot), z\big) \in L^2(B),$$
$$\tilde{\varphi}_{t,s}(\cdot, z) := \varphi_{t,s}\big(\phi(s, \cdot), z\big) \in H^{\frac{1}{2}}(\partial D),$$

and a real coupling parameter $\rho \neq 0$. Then we deduce the following theorem.

Theorem 2.1. *A combined potential $u_{t,s}(\cdot, z) \in L^2_{loc}(\mathbb{R}^2\backslash(\{z\} \cup \bar{D}_s))$ of the form (2.7) is a solution of (2.5) if $\tilde{u}_{t,s}|_B(\cdot, z) \in L^2(B)$ and $\tilde{\varphi}_{t,s}(\cdot, z) \in H^{1/2}(\partial D)$ satisfy the following system of integral equations:*

$$\tilde{u}_{t,s}|_B + (\tilde{K}_{t,s} - i\rho\tilde{S}_{t,s})\tilde{\varphi}_{t,s} + \eta T_t\tilde{u}_{t,s}|_B = \tilde{G}_{R,t} \quad \text{in } B, \tag{2.8a}$$
$$\tilde{\varphi}_{t,s} + (K_s - i\rho S_s)\tilde{\varphi}_{t,s} + 2\eta\tilde{T}_{t,s}\tilde{u}_{t,s}|_B = 2\tilde{G}_{R,s} \quad \text{on } \partial D, \tag{2.8b}$$

where $\tilde{G}_{R,t}(\cdot, z) := G_R(\psi(\cdot, t), z)$ and $\tilde{G}_{R,s}(\cdot, z) := G_R(\phi(\cdot, s), z)$.

Proof. A simple calculation shows that $u_{t,s}$ defined by (2.7) satisfies $\Delta u_{t,s} + \kappa_t^2 u_{t,s} = 0$ in $\mathbb{R}^2\backslash(\{z\} \cup \bar{D}_s)$. Since G_R satisfies the Sommerfeld radiation condition, $u_{t,s}$ also satisfies the Sommerfeld radiation condition. Restricting (2.7) to B_t gives the Eq. (2.8a), and the Eq. (2.8a) can also be extended to (2.7). For the Dirichlet boundary condition, we can use the jump relation(cf. [12]) of the potential operator to deduce

$$u_{t,s}(\cdot, z)|_+ = G_R(\cdot, z) - \frac{1}{2}(K_s - i\rho S_s + I)\tilde{\varphi}_{t,s}(\cdot, z) - \eta\tilde{T}_{t,s}\tilde{u}_{t,s}|_B(\cdot, z) = 0,$$

where $\cdot|_\pm$ indicating the limits of $\cdot$ from the outside and inside of ∂D_s. □

We define $\boldsymbol{M}_{t,s} : L^2(B) \times H^{1/2}(\partial D) \mapsto L^2(B) \times H^{1/2}(\partial D)$ by

$$\boldsymbol{M}_{t,s} := \begin{pmatrix} \eta T_t & \tilde{K}_{t,s} - i\rho\tilde{S}_{t,s} \\ 2\eta\tilde{T}_{t,s} & K_s - i\rho S_s \end{pmatrix}.$$

Then the system of integral equations (2.8) can be written as

$$\{\boldsymbol{I} + \boldsymbol{M}_{t,s}\} \begin{pmatrix} \tilde{u}_{t,s}|_B \\ \tilde{\varphi}_{t,s} \end{pmatrix} = \begin{pmatrix} \tilde{G}_{R,t}|_B \\ 2\tilde{G}_{R,s}|_{\partial D} \end{pmatrix}. \tag{2.9}$$

Theorem 2.2. *There is a unique solution to* (2.9) *such that*

$$\left\| \begin{pmatrix} \tilde{u}_{t,s}|_B(\cdot, z) \\ \tilde{\varphi}_{t,s}(\cdot, z) \end{pmatrix} \right\|_{L^2(B)\times H^{1/2}(\partial D)} \leq C \left\| \begin{pmatrix} \tilde{G}_{R,t}|_B(\cdot, z) \\ 2\tilde{G}_{R,s}|_{\partial D}(\cdot, z) \end{pmatrix} \right\|_{L^2(B)\times H^{1/2}(\partial D)},$$

where $C = C(B, D, \kappa)$ is a positive constant.

Proof. Note that all elements of $\boldsymbol{M}_{t,s}$ are weak singular-type operators, leading to that $\boldsymbol{M}_{t,s}$ is a compact operator. Thus, the existence of the solution to (2.9) follows from the uniqueness by the Riesz-Fredholm theory. Consider the following homogeneous problem:

$$\begin{aligned} &\tilde{u}_{t,s}|_B + (\tilde{K}_{t,s} - i\rho\tilde{S}_{t,s})\tilde{\varphi}_{t,s} + \eta T_t\tilde{u}_{t,s}|_B = 0 \quad \text{in } B, \\ &\tilde{\varphi}_{t,s} + (K_s - i\rho S_s)\tilde{\varphi}_{t,s} + 2\eta\tilde{T}_t\tilde{u}_{t,s}|_B = 0 \qquad \text{on } \partial D. \end{aligned}$$

We first have $\tilde{u}_{t,s} = 0$ in $\mathbb{R}^2\backslash\bar{D}$ from the uniqueness (cf. [45]) of (2.5), which $\tilde{u}_{t,s}|_B = 0$ follows. Using the jump relation of the potential operator yields

$$u_{t,s}|_- = \varphi_{t,s}, \quad \left.\frac{\partial u_{t,s}}{\partial \nu_s}\right|_- = i\rho\varphi_{t,s} \quad \text{on } \partial D_s,$$

where $\cdot|_\pm$ indicating the limits of $\cdot$ from the outside and inside of ∂D_s. Finally, using Green's theorem, we obtain

$$i\rho\int_{\partial D_s} |\varphi_{t,s}|^2 \,\mathrm{ds}(x) = \int_{\partial D_s} \bar{u}_{t,s}|_- \left.\frac{\partial u_{t,s}}{\partial \nu_s}\right|_- \mathrm{ds}(x) = \int_{D_s} \left\{ |\operatorname{grad} u_{t,s}|^2 - \kappa_2^2 |u_{t,s}|^2 \right\} \mathrm{d}x,$$

which gives $\tilde{\varphi}_{t,s}(\cdot, z) = 0$ on ∂D by taking the imaginary part for both sides of the equation. It is easy to see that the operators in $\boldsymbol{M}_{t,s}$ are related to B, D and κ, so the corresponding constant C depends on B, D, and κ. The proof is complete. □

Then the total field to the perturbation problem (2.5) can be expressed as

$$u_{t,s}(x, z) = P_{t,s}(I + \boldsymbol{M}_{t,s})^{-1} R_{t,s} G_R(x, z) \quad \text{in } \mathbb{R}^2\backslash(\bar{D}_s \cup z),$$

where

$$
\begin{aligned}
&P_{t,s} : L^2(B) \times H^{\frac{1}{2}}(\partial D) \ \rightarrow \ H^1_{loc}\big(\mathbb{R}^2 \backslash (\{z\} \cup \bar{D}_s)\big),\\
&P_{t,s}\begin{pmatrix}\psi\\ \varphi\end{pmatrix}(x,z) = G_R(x,z) - \eta \int_B G_R(x,y_t)|J(t,y)|\psi(y,z)\,\mathrm{d}y\\
&\qquad\qquad - \int_{\partial D}\left\{\frac{\partial G_R(x,y_s)}{\partial \nu_s(y_s)} - i\rho G_R(x,y_s)\right\}|\mathscr{J}(s,y)|\varphi(y,z)\,\mathrm{ds}(y),\\
&R_{t,s} : H^1(Q) \ \rightarrow \ L^2(B) \times H^{\frac{1}{2}}(\partial D),\\
&R_{t,s}G_R(x,z) = \begin{pmatrix} G_R(x_t,z)\\ 2G_R(x_s,z)\end{pmatrix}.
\end{aligned}
$$

Here, Q is a bounded set in $\mathbb{R}^2$ containing B and D.

3. Shape Derivative

In this section, we will prove the existence of shape derivatives corresponding to the total field, which can be characterized as a solution to a special scattering problem.

3.1. Shape derivative of each operator

In this subsection, we will calculate shape derivatives of each operator. We first deal with

$$
\begin{aligned}
K_s\varphi(x) =& \ 2\int_{\partial D}\frac{\partial G_R(x_s,y_s)}{\partial \nu_s(y_s)}|\mathscr{J}(s,y)|\varphi(y)ds(y)\\
=& \int_{\partial D}\langle \nu_s(y_s), y_s - x_s\rangle\left\{h_1(|x_s-y_s|)\frac{\log(|x_s-y_s|)}{|x_s-y_s|} + \frac{h_2(|x_s-y_s|)}{|x_s-y_s|^2}\right\}|\mathscr{J}(s,y)|\varphi(y)\mathrm{ds}(y)\\
=:& \int_{\partial D} F_{K,s}(x,y)\varphi(y)\mathrm{d}s(y),
\end{aligned}
$$

where h_1 and h_2 are both analytic functions.

Lemma 3.1. *$F_{K,s}(x,y)$ is second order differentiable with respect to s at $s=0$ and the operators with kernel functions $\partial_s F_{K,0}(x,y)$ and $\partial_s^2 F_{K,0}(x,y)$ are compact from $H^{1/2}(\partial D)$ to $H^{1/2}(\partial D)$.*

Proof. We will divide the proof into three steps.

Step 1. Firstly, we define three functions as

$$
f_{x,y}(s) := x_s - y_s, \quad f_{1,x,y}(s) := |x_s - y_s|, \quad f_{2,x,y}(s) := \frac{1}{|x_s - y_s|^n}, \quad \forall\, x \neq y, \quad x, y \in \partial D.
$$

A direct calculation shows that their derivatives are given by

$$
\begin{aligned}
&f'_{x,y}(0) = \mathscr{V}(x) - \mathscr{V}(y),\\
&f'_{1,x,y}(0) = \frac{1}{|x-y|}\big\langle (x-y), \big(\mathscr{V}(x) - \mathscr{V}(y)\big)\big\rangle,\\
&f'_{2,x,y}(0) = -n\frac{1}{|x-y|^{n+2}}\big\langle (x-y), \big(\mathscr{V}(x) - \mathscr{V}(y)\big)\big\rangle.
\end{aligned}
$$

From the continuity of $\mathscr{V}(\cdot)$, it is deduced that $|\mathscr{V}(x)-\mathscr{V}(y)|\le C_1|x-y|$, which leads to $|f'_{1,x,y}(0)|\le C_2|x-y|$ and $|f'_{2,x,y}(0)|\le C_3/|x-y|^n$. Here, C_i are positive constants. Similarly, we can directly compute

$$\begin{aligned} f''_{1,x,y}(0) &= -\frac{1}{|x-y|^3}\big\langle (x-y), \big(\mathscr{V}(x)-\mathscr{V}(y)\big)\big\rangle^2 \\ &\quad + \frac{1}{|x-y|}\big\langle \big(\mathscr{V}(x)-\mathscr{V}(y)\big), \big(\mathscr{V}(x)-\mathscr{V}(y)\big)\big\rangle \\ &\quad + \frac{1}{|x-y|}\big\langle (x-y), \big(\mathscr{U}(x)-\mathscr{U}(y)\big)\big\rangle, \end{aligned} \tag{3.1}$$

$$f''_{2,x,y}(0) = n(n+1)\frac{1}{|x-y|^{n+2}}\big(f'_{1,x,y}(0)\big)^2 - n\frac{1}{|x-y|^{n+1}}f''_{1,x,y}(0). \tag{3.2}$$

With the help of $|\mathscr{U}(x)-\mathscr{U}(y)|\le C_4|x-y|$, (3.1) and (3.2) lead to $|f''_{1,x,y}(0)|\le C_5|x-y|$ and $|f''_{2,x,y}(0)|\le C_6/|x-y|^n$.

Define $f_{3,x,y}(s) := \log|x_s-y_s|$ for any $x\neq y$ and $x,y\in\partial D$, which first and second order derivatives are given as

$$\begin{aligned} f'_{3,x,y}(0) &= \frac{1}{|x-y|^2}\big\langle (x-y), \big(\mathscr{V}(x)-\mathscr{V}(y)\big)\big\rangle, \\ f''_{3,x,y}(0) &= -2\frac{1}{|x-y|^4}\big\langle (x-y), \big(\mathscr{V}(x)-\mathscr{V}(y)\big)\big\rangle^2 \\ &\quad + \frac{1}{|x-y|^2}\big\langle \big(\mathscr{V}(x)-\mathscr{V}(y)\big), \big(\mathscr{V}(x)-\mathscr{V}(y)\big)\big\rangle \\ &\quad + \frac{1}{|x-y|^2}\big\langle (x-y), \big(\mathscr{U}(x)-\mathscr{U}(y)\big)\big\rangle. \end{aligned}$$

Then, one has estimates $|f'_{3,x,y}(0)|\le C_7$ and $|f''_{3,x,y}(0)|\le C_8$.

Step 2. Suppose that $x=x(s_1), y=y(s_2)$ are local coordinates on ∂D. Naturally, we have $x_s(s_1)=\phi(s,x(s_1))$ and $y_s(s_2)=\phi(s,y(s_2))$. Notice $x=(x_1,x_2), y=(y_1,y_2), \phi=(\phi_1,\phi_2)$, $\mathscr{V}=(\mathscr{V}_1,\mathscr{V}_2)$ and $\mathscr{U}=(\mathscr{U}_1,\mathscr{U}_2)$. Then,

$$g(s) := \langle \boldsymbol{v}_s(y_s), x_s-y_s\rangle = \frac{\big\langle \big(\partial\phi_2\big(s,y(s_2)\big)/\partial s_2, -\partial\phi_1\big(s,y(s_2)\big)/\partial s_2\big), x_s(s_1)-y_s(s_2)\big\rangle}{f_{4,y}(s)},$$

where

$$f_{4,y}(s) := \sqrt{\left(\frac{\partial\phi_1}{\partial s_2}\big(s,y(s_2)\big)\right)^2 + \left(\frac{\partial\phi_2}{\partial s_2}\big(s,y(s_2)\big)\right)^2}.$$

It is easy to check that there exist constants $C_9, C_{10}>0$ such that $0<C_9\le f_{4,y}(0)\le C_{10}$. For $f_{4,y}(s)$, we also have

$$f'_{4,y}(0) = \frac{\partial y_1(s_2)/\partial s_2\cdot\partial\mathscr{V}_1\big(y(s_2)\big)/\partial s_2 + \partial y_2(s_2)/\partial s_2\cdot\partial\mathscr{V}_2\big(y(s_2)\big)/\partial s_2}{\sqrt{\big(\partial y_1(s_2)/\partial s_2\big)^2+\big(\partial y_2(s_2)/\partial s_2\big)^2}},$$

which leads to $|f'_{4,y}(0)|\le C_{11}$. Furthermore, we can compute its second order derivative

$$f''_{4,y}(0) = \frac{\big(\partial\mathscr{V}_1\big(y(s_2)\big)/\partial s_2\big)^2+\big(\partial\mathscr{V}_2\big(y(s_2)\big)/\partial s_2\big)^2}{\sqrt{\big(\partial y_1(s_2)/\partial s_2\big)^2+\big(\partial y_2(s_2)/\partial s_2\big)^2}}$$

$$+\frac{\partial y_1(s_2)/\partial s_2\cdot\partial\mathscr{U}_1\big(y(s_2)\big)/\partial s_2+\partial y_2(s_2)/\partial s_2\cdot\partial\mathscr{U}_2\big(y(s_2)\big)/\partial s_2}{\sqrt{\big(\partial y_1(s_2)/\partial s_2\big)^2+\big(\partial y_2(s_2)/\partial s_2\big)^2}}$$
$$-\frac{\big(\partial y_1(s_2)/\partial s_2\cdot\partial\mathscr{V}_1\big(y(s_2)\big)/\partial s_2+\partial y_2(s_2)/\partial s_2\cdot\partial\mathscr{V}_2\big(y(s_2)\big)/\partial s_2\big)^2}{\big(\big(\partial y_1(s_2)/\partial s_2\big)^2+\big(\partial y_2(s_2)/\partial s_2\big)^2\big)^{3/2}},$$

which also implies that $|f''_{4,y}(0)|\le C_{12}$. We denote

$$h(s):=\left\langle\left(\frac{\partial\phi_2}{\partial s_2}\big(s,y(s_2)\big),-\frac{\partial\phi_1}{\partial s_2}\big(s,y(s_2)\big)\right),\big(x_s(s_1)-y_s(s_2)\big)\right\rangle.$$

Following the above preparation, it is easy to deduce that $g(0),g'(0),g''(0)$ and $h(0)$, $h'(0)$, $h''(0)$ have the same singularity, respectively.

We compute the first, second order derivative of $h(s)$ as

$$\begin{aligned}h'(0)=&\left\langle\left(\frac{\partial\mathscr{V}_2\big(y(s_2)\big)}{\partial s_2},-\frac{\partial\mathscr{V}_1\big(y(s_2)\big)}{\partial s_2}\right),\big(x(s_1)-y(s_2)\big)\right\rangle\\&+\left\langle\left(\frac{\partial y_2(s_2)}{\partial s_2},-\frac{\partial y_1(s_2)}{\partial s_2}\right),\big(\mathscr{V}\big(x(s_1)\big)-\mathscr{V}\big(y(s_2)\big)\big)\right\rangle,\\h''(0)=&\left\langle\left(\frac{\partial\mathscr{U}_2\big(y(s_2)\big)}{\partial s_2},-\frac{\partial\mathscr{U}_1\big(y(s_2)\big)}{\partial s_2}\right),\big(x(s_1)-y(s_2)\big)\right\rangle\\&+\left\langle\left(\frac{\partial y_2(s_2)}{\partial s_2},-\frac{\partial y_1(s_2)}{\partial s_2}\right),\big(\mathscr{U}\big(x(s_1)\big)-\mathscr{U}\big(y(s_2)\big)\big)\right\rangle\\&+2\left\langle\left(\frac{\partial\mathscr{V}_2\big(y(s_2)\big)}{\partial s_2},-\frac{\partial\mathscr{V}_1\big(y(s_2)\big)}{\partial s_2}\right),\big(\mathscr{V}\big(x(s_1)\big)-\mathscr{V}\big(y(s_2)\big)\big)\right\rangle,\end{aligned}$$

which shows that $h(0),h'(0)$ and $h''(0)$ have the same singularity.

Step 3. By assumption, $|\mathscr{J}(s,y)|$ and its first and second order derivative with respect to s are bounded at $s=0$. Following the singularity analysis in Steps 1-2, one has that K_s is a bounded operator from $H^{1/2}(\partial D)$ to $H^{3/2}(\partial D)$. The proof is complete. □

We also have the following Lemma for $F_{K,s}(x,y)$.

Lemma 3.2.

$$\lim_{s\to0}\frac{1}{s}\left[\int_{\partial D}\big(F_{K,s}(x,y)-F_{K,0}(x,y)\big)\varphi(y)\,\mathrm{ds}(y)\right]=\int_{\partial D}\partial_sF_{K,0}(x,y)\varphi(y)\,\mathrm{ds}(y)$$

in the sense of $\mathcal{L}(H^{1/2}(\partial D),H^{1/2}(\partial D))$.

Proof. From Taylor's formula, we have

$$F_{K,s_0}(x,y)-F_{K,0}(x,y)=s_0\partial_sF_{k,0}(x,y)+s_0^2\int_0^1(1-\alpha)\partial_s^2F_{K,s_0\alpha}(x,y)\mathrm{d}\alpha$$

for $s_0>0$. Using the Fubini-Tonelli's theorem yields

$$\left\|\int_{\partial D}\left(\int_0^1(1-\alpha)\partial_s^2F_{K,s_0\alpha}(x,y)\mathrm{d}\alpha\right)\varphi(y)\,\mathrm{ds}(y)\right\|_{H^{1/2}(\partial D)}$$

$$= \left\| \int_0^1 (1-\alpha) \left(\int_{\partial D} \partial_s^2 F_{K,s_0\alpha}(x,y)\varphi(y)\,\mathrm{ds}(y) \right) \mathrm{d}\alpha \right\|_{H^{1/2}(\partial D)}$$

$$\leq \sup_{\alpha\in[0,1]} \left\| \int_{\partial D} \partial_s^2 F_{K,s_0\alpha}(x,y)\varphi(y)\,\mathrm{ds}(y) \right\|_{H^{1/2}(\partial D)} \leqslant C\|\varphi\|_{H^{1/2}(\partial D)}.$$

Therefore,

$$\varphi \;\mapsto\; \int_{\partial D} \int_0^1 (1-\alpha)\partial_s^2 F_{K,s_0\alpha}(x,y)\varphi(y)\mathrm{d}\alpha\mathrm{ds}(y)$$

is a bounded linear operator from $H^{1/2}(\partial D)$ to $H^{1/2}(\partial D)$. Finally,

$$\left\| \frac{1}{s_0} \left(\int_{\partial D} F_{K,s_0}(x,y)\varphi(y)\mathrm{ds}(y) - \int_{\partial D} F_{K,0}(x,y)\varphi(y)\,\mathrm{ds}(y) \right) \right.$$
$$\left. - \int_{\partial D} \partial_s F_{K,0}(x,y)\varphi(y)\,\mathrm{ds}(y) \right\|_{H^{1/2}(\partial D)}$$
$$= \left\| s_0 \int_{\partial D} \int_0^1 (1-\alpha)\partial_s^2 F_{K,s_0\alpha}(x,y)\varphi(y)\mathrm{d}\alpha\,\mathrm{ds}(y) \right\|_{H^{1/2}(\partial D)} \;\to\; 0 \quad \text{as} \quad s_0 \;\to\; 0.$$

The proof is complete. □

We easily obtain the following theorem by Lemmas 3.1-3.2.

Theorem 3.1. *The operator* $s \in [0,S) \mapsto K_s \in \mathcal{L}(H^{1/2}(\partial D), H^{1/2}(\partial D))$ *is differentiable at* $s = 0$ *with*

$$\partial_s K_0\varphi(x) = \int_{\partial D} \partial_s F_{K,0}(x,y)\varphi(y)\,\mathrm{ds}(y).$$

Remark 3.1. Following the lines of K_s, it can be shown that $S_s, T_t, \tilde{S}_{t,s}, \tilde{K}_{t,s}, \tilde{T}_{t,s}$ and $P_{t,s}$ are differentiable with respect to t and s at 0, respectively. Then, the matrix operator $\boldsymbol{M}_{t,s}$ consisting of the above partial operators is differentiable with respect to t and s at $(t,s) = (0,0)$.

Moreover, the differentiability of $R_{t,s}$ can be proved via chain rule and the vector derivation rule with

$$\partial_s R_{0,0}G_R(x,z) = \begin{pmatrix} 0 \\ 2\nabla_x G_R(x,z)\cdot \mathscr{V}(x) \end{pmatrix},$$
$$\partial_t R_{0,0}G_R(x,z) = \begin{pmatrix} \nabla_x G_R(x,z)\cdot \boldsymbol{V}(x) \\ 0 \end{pmatrix}.$$

3.2. Shape derivative of the total field

Based on the preparation of the previous subsection, we can obtain the differentiability theorem of the total field with respect to t and s at $(t,s) = (0,0)$.

Theorem 3.2. *Let* $u_{t,s}$ *be a solution of* (2.5)*, then*

$$(t,s) \in [0,T)\times[0,S) \;\mapsto\; u_{t,s} \in H^1_{loc}\big(\mathbb{R}^2\backslash(\{z\}\cup\bar{D}_s)\big)$$

is differentiable with respect to t *and* s *at* $(t,s) = (0,0)$ *with*

$$\partial_s u_{0,0}(x,z) = \partial_s P_{0,0}\left(I+\boldsymbol{M}_{0,0}\right)^{-1} R_{0,0}G_R(x,z) + P_{0,0}\left(I+\boldsymbol{M}_{0,0}\right)^{-1}\partial_s R_{0,0}G_R(x,z)$$
$$- P_{0,0}\left(I+\boldsymbol{M}_{0,0}\right)^{-1}\partial_s \boldsymbol{M}_{0,0}\left(I+\boldsymbol{M}_{0,0}\right)^{-1} R_{0,0}G_R(x,z),$$
$$\partial_t u_{0,0}(x,z) = \partial_t P_{0,0}\left(I+\boldsymbol{M}_{0,0}\right)^{-1} R_{0,0}G_R(x,z) + P_{0,0}\left(I+\boldsymbol{M}_{0,0}\right)^{-1}\partial_t R_{0,0}G_R(x,z)$$
$$- P_{0,0}\left(I+\boldsymbol{M}_{0,0}\right)^{-1}\partial_t \boldsymbol{M}_{0,0}\left(I+\boldsymbol{M}_{0,0}\right)^{-1} R_{0,0}G_R(x,z).$$

Proof. Using the derivation formula for the inverse operator (cf. [39]), one obtains

$$\partial_t(I+\boldsymbol{M}_{0,0})^{-1} = -(I+\boldsymbol{M}_{0,0})^{-1}\partial_t\boldsymbol{M}_{t,s}(I+\boldsymbol{M}_{0,0})^{-1},$$
$$\partial_s(I+\boldsymbol{M}_{0,0})^{-1} = -(I+\boldsymbol{M}_{0,0})^{-1}\partial_s\boldsymbol{M}_{t,s}(I+\boldsymbol{M}_{0,0})^{-1}.$$

The assertion can be shown by using the chain rule and the differentiability of each operator. The proof is complete. □

3.3. Characterization of the derivations

For this section, we will give a characterization of the shape derivatives of the total field. Since the incident field is independent of t and s, the scattered field has the same shape derivative with the total field.

Theorem 3.3. *Suppose that $u \in H^1_{loc}(\mathbb{R}^2\backslash(\{z\}\cup\bar{D}))$ is the solution to (2.1)-(2.3). Then total field $u_{t,s}$ has shape derivatives with respect to t and s at $(t,s)=(0,0)$, denoted by u'_t and u'_s, and $u'_t \in H^1_{loc}(\mathbb{R}^2\backslash\bar{D})$ is a solution of*

$$\begin{cases} \Delta u'_t + \kappa_1^2 u'_t = 0 & \text{in } \Omega_1,\\ \Delta u'_t + \kappa_2^2 u'_t = 0 & \text{in } \Omega_2,\\ u'_t|_+ - u'_t|_- = 0 & \text{on } \Gamma,\\ \dfrac{\partial u'_t}{\partial\nu}\Big|_+ - \dfrac{\partial u'_t}{\partial\nu}\Big|_- = (\boldsymbol{V}\cdot\nu)\big(\kappa_2^2-\kappa_1^2\big)u & \text{on } \Gamma,\\ u'_t = 0 & \text{on } \partial D,\\ \lim\limits_{r\to\infty}\sqrt{r}\left(\dfrac{\partial u_t^{\mathrm{s}\prime}}{\partial r} - \mathrm{i}\kappa u_t^{\mathrm{s}\prime}\right) = 0, & r=|x|, \end{cases} \tag{3.3}$$

and $u'_s \in H^1_{loc}(\mathbb{R}^2\backslash\bar{D})$ is a solution of

$$\begin{cases} \Delta u'_s + \kappa^2 u'_s = 0 & \text{in } \mathbb{R}^2\backslash\bar{D},\\ u'_s = -(\mathscr{V}\cdot\nu)\dfrac{\partial u}{\partial\nu} & \text{on } \partial D,\\ \lim\limits_{r\to\infty}\sqrt{r}\left(\dfrac{\partial u_s^{\mathrm{s}\prime}}{\partial r} - \mathrm{i}\kappa u_s^{\mathrm{s}\prime}\right) = 0, & r=|x|. \end{cases} \tag{3.4}$$

Proof. The existence of u'_t and u'_s follows from Theorem 3.2. So we just need to verify that u'_t and u'_s satisfies (3.3) and (3.4), respectively. For convenience, we denote $\varphi := \varphi_{0,0}$ and $u := u_{0,0}$.

Firstly, we verify that u'_t satisfies Eq. (3.3). From the Definition 2.3 and [16, Corollary 5.2.5], we have

$$\begin{aligned} u'_t(x,z) = &-\eta\int_B G_R(x,y)u'_t(y,z)\,\mathrm{d}y - \eta\int_{\tilde{\Gamma}_R} G_R(x,y)\boldsymbol{V}\cdot\nu(y)u(y,z)\,\mathrm{ds}(y)\\ &-\int_{\partial D}\left\{\frac{\partial G_R(x,y)}{\partial\nu(y)} - i\rho G_R(x,y)\right\}\varphi'_t(y,z)\,\mathrm{ds}(y), \quad x\in\mathbb{R}^2\backslash\bar{D}, \end{aligned} \tag{3.5}$$

where $\varphi'_t(y,z)$ is the derivative of $\varphi_{t,0}(y,z)$ with respect to t at $(t,s)=(0,0)$. With the integral representation (3.5) of $u'_t(\cdot,z)$, it is easy to show that $u'_t(\cdot,z)$ satisfies $\Delta u'_t(\cdot,z)+\kappa_1^2 u'_t(\cdot,z)=0$

in Ω_1 and $\Delta u_t'(\cdot,z)+\kappa_2^2 u_t'(\cdot,z)=0$ in Ω_2. Since G_R satisfies the Sommerfeld radiation condition, $u_t'(\cdot,z)$ also satisfies the Sommerfeld radiation condition. So we just need to verify that u_t' satisfies the corresponding boundary conditions on Γ and ∂D.

Now, we differentiate both sides of the Eq. (2.9) with respect to t to obtain

$$2\eta\tilde{T}_{0,0}u_t'(x,z)+(K_0-i\rho S_0)\varphi_t'(x,z)+\eta S_{\tilde{\Gamma}_R}\big((\boldsymbol{V}\cdot\nu)u\big)(x,z)+\varphi_t'(x,z)=0$$

for $x\in\partial D$, where

$$S_{\tilde{\Gamma}_R}\varphi(x):=2\int_{\tilde{\Gamma}_R}G_R(x,y)\varphi(y)\,\mathrm{ds}(y),\quad x\in\partial D.$$

From the integral representation (3.5) and the jump relations of the potential operators at the boundary Γ and ∂D, it follows that

$$\begin{cases} u_t'|_+-u_t'|_-=0 & \text{on } \Gamma,\\ \dfrac{\partial u_t'}{\partial\nu}\Big|_+-\dfrac{\partial u_t'}{\partial\nu}\Big|_-=(\boldsymbol{V}\cdot\nu)\big(\kappa_2^2-\kappa_1^2\big)u & \text{on } \Gamma,\\ u_t'=-\eta\tilde{T}_{0,0}u_t'-\dfrac{1}{2}(K_0-i\rho S_0)\varphi_t'-\dfrac{\eta}{2}S_{\tilde{\Gamma}_R}\big((\boldsymbol{V}\cdot\nu)u\big)-\dfrac{1}{2}\varphi_t'=0 & \text{on } \partial D. \end{cases}$$

Next, we will verify that u_s' satisfies (3.4). It follows from [16, Proposition 5.4.18] that

$$\begin{aligned} u_s'(x,z)=&-\eta\int_B G_R(x,y)u_s'(y,z)\,\mathrm{d}y-\int_{\partial D}\frac{\partial G_R(x,y)}{\partial\nu(y)}\tilde{\varphi}_s'(y,z)\,\mathrm{ds}(y)\\ &+\kappa_2^2\int_{\partial D}G_R(x,y)\varphi(y,z)\mathscr{V}\cdot\nu(y)\,\mathrm{ds}(y)+i\rho\int_{\partial D}G_R(x,y)\tilde{\varphi}_s'(y,z)\,\mathrm{ds}(y)\\ &+i\rho\int_{\partial D}\left\{G_R(x,y)H_{\partial D}+\frac{\partial G_R(x,y)}{\partial\nu(y)}\right\}\varphi(y,z)\mathscr{V}\cdot\nu(y)\,\mathrm{ds}(y) \end{aligned}\tag{3.6}$$

for $x\in\mathbb{R}^2\backslash\bar{D}$, and

$$\begin{aligned} &\tilde{\varphi}_s'(x,z)+2\eta\tilde{T}_{0,0}u_s'(x,z)+K_0\tilde{\varphi}'(x,z)-\kappa_2^2S_0(\mathscr{V}\cdot\nu\varphi)(x,z)\\ &\quad-i\rho\{S_0(\tilde{\varphi}_s'+H_{\partial D}\mathscr{V}\cdot\nu\varphi)(x,z)+K_0(\mathscr{V}\cdot\nu\varphi)(x,z)\}\mathscr{V}\\ &\quad\times\nu(x)\{2\eta Nu(x,z)+(\mathcal{T}-i\rho K')\varphi(x,z)\}\\ &=2\frac{\partial G_R(x,z)}{\partial\nu(x)}\mathscr{V}\cdot\nu(x) \end{aligned}$$

for $x\in\partial D$, where $\tilde{\varphi}_s'(y,z)$ is the derivative of $\varphi_{0,s}(y_s,z)$ with respect to s at $(t,s)=(0,0)$, $H_{\partial D}$ is the mean curvature of ∂D, and

$$\begin{aligned} Nu(x,z)&:=\frac{\partial}{\partial\nu(x)}\int_B G_R(x,y)u(y,z)\,\mathrm{ds}(y), && x\in\partial D,\\ K'\varphi(x,z)&:=2\frac{\partial}{\partial\nu(x)}\int_{\partial D}G_R(x,y)\varphi(y,z)\,\mathrm{ds}(y), && x\in\partial D,\\ \mathcal{T}\varphi(x,z)&:=2\frac{\partial}{\partial\nu(x)}\int_{\partial D}\frac{\partial G_R(x,y)}{\partial\nu(y)}\varphi(y,z)\,\mathrm{ds}(y), && x\in\partial D. \end{aligned}$$

Similar to u_t', it is easily checked that u_s' satisfies the Helmholtz equations and Sommerfeld radiation conditions. The left is to verify that u_s' satisfies the boundary conditions. Let x

converge to ∂D from the outside of D, we have

$$\begin{aligned}
u_s'(x,z) &= -\frac{1}{2}\tilde{\varphi}_s'(x,z) + \frac{i\rho}{2}\mathscr{V}\cdot\nu(x)\varphi(x,z) - \eta\tilde{T}_{0,0}u_s'(x,z) - \frac{1}{2}K_0\tilde{\varphi}_s'(x,z) \\
&\quad + \frac{\kappa_2^2}{2}S_0(\mathscr{V}\cdot\nu\varphi)(x,z) + \frac{i\rho}{2}\big\{S_0(\tilde{\varphi}_s' + H_{\partial D}\mathscr{V}\cdot\nu\varphi)(x,z) + K_0(\mathscr{V}\cdot\nu\varphi)(x,z)\big\} \\
&= -\frac{\partial G_R(x,y)}{\partial\nu(x)}\mathscr{V}\cdot\nu(x) + \mathscr{V}\cdot\nu(x)\bigg\{\eta N u(x,z) + \frac{1}{2}\big(\mathcal{T} - i\rho(K'-I)\big)\varphi(x,z)\bigg\} \\
&= -(\mathscr{V}\cdot\nu)(x)\frac{\partial u(x,z)}{\partial\nu(x)}, \quad x\in\partial D,
\end{aligned}$$

which leads to

$$\begin{cases}
u_s'|_+ - u_s'|_- = 0 & \text{on } \Gamma, \\
\dfrac{\partial u_s'}{\partial\nu}\bigg|_+ - \dfrac{\partial u_s'}{\partial\nu}\bigg|_- = 0 & \text{on } \Gamma, \\
u_s' = -(\mathscr{V}\cdot\nu)\dfrac{\partial u}{\partial\nu} & \text{on } \partial D.
\end{cases}$$

The proof is complete. □

4. Numerical Method

Using the shape derivatives established in Theorem 3.3, we propose in this section a Newton-type algorithm for the simultaneous recovery of the infinite rough interface Γ and the impenetrable obstacles D. More precisely, we will use the scattered field data u^s on Γ_{mea} to recover infinite interfaces and bounded obstacles. To make the results more accurate we will also use multi-frequency scattered field data.

Denote u_κ^s as the scattered field in (2.1)-(2.3) with κ as the wavenumber, and we characterize the infinite interface Γ by the function $f \in C_0^2(\mathbb{R})$ and the bounded obstacles D by $g \in C^2([0,2\pi],\mathbb{R}^2)$. Let $\mathcal{F}_\kappa : C_0^2(\mathbb{R})\times C^2([0,2\pi],\mathbb{R}^2) \to L^2(\Gamma_{mea})$ be the scattered field operator, which maps f and g to the scattered field $u_\kappa^s|_{\Gamma_{mea}}$, that is,

$$\mathcal{F}_\kappa[f,g](x) = u_\kappa^s|_{\Gamma_{mea}}. \tag{4.1}$$

Since $\mathcal{F}_\kappa$ is differentiable at both f and g, we can solve for f and g from Eq. (4.1) by Newton-type iterative methods. Assume that $f_\kappa^{app}$and g_κ^{app} are approximate functions of each fixed wavenumber $\kappa > 0$ respectively. We consider the linearized equation of Eq. (4.1)

$$\begin{aligned}
&\big(\mathcal{F}_\kappa\big[f_\kappa^{app}, g_\kappa^{app}\big]\big)(x) + \big(\mathcal{F}'_{\kappa,f}\big[f_\kappa^{app}, g_\kappa^{app}; \theta_f\big]\big)(x) \\
&\quad + \big(\mathcal{F}'_{\kappa,g}\big[f_\kappa^{app}, g_\kappa^{app}; \theta_g\big]\big)(x) = u_\kappa^s|_{\Gamma_{mes}},
\end{aligned} \tag{4.2}$$

where θ_f and θ_g are the update functions to be determined.

By Theorem 3.3,

$$\begin{aligned}
&\mathcal{F}'_{\kappa,f}[f_\kappa^{app}, g_\kappa^{app}; \theta_f](x) := u_t'|_{\Gamma_{mea}}, \quad \theta_f \in C_0^2 \quad (\Gamma_{f^{app}}), \\
&\mathcal{F}'_{\kappa,g}[f_\kappa^{app}, g_\kappa^{app}; \theta_g](x) := u_s'|_{\Gamma_{mea}}, \quad \theta_g \in C^2 \quad ([0,2\pi],\mathbb{R}^2)
\end{aligned}$$

are solutions of two forward scattering problems (3.3) and (3.4), where they satisfy the boundary conditions

$$\begin{cases} u_t'|_+ - u_t'|_- = 0 & \text{on } \Gamma_{f^{app}}, \\ \left.\dfrac{\partial u_t'}{\partial \nu}\right|_+ - \left.\dfrac{\partial u_t'}{\partial \nu}\right|_- = \big((t,\theta_f(t))^\top \cdot \nu\big)(\kappa_2^2 - \kappa_1^2)u & \text{on } \Gamma_{f^{app}}, \\ u_t' = 0 & \text{on } \partial D_{f^{app}}, \end{cases}$$

and

$$\begin{cases} u_s'|_+ - u_s'|_- = 0 & \text{on } \Gamma_{g^{app}}, \\ \left.\dfrac{\partial u_s'}{\partial \nu}\right|_+ - \left.\dfrac{\partial u_s'}{\partial \nu}\right|_- = 0 & \text{on } \Gamma_{g^{app}}, \\ u_s' = -(\theta_g \cdot \nu)\dfrac{\partial u}{\partial \nu} & \text{on } \partial D_{g^{app}}. \end{cases}$$

For the constant $c > 0$, define the function space B_c by

$$B_c := \big\{ f \in C^2(\mathbb{R}) \,:\, \|f\|_{C^2(\mathbb{R})} \le c,\ f(s) = 0 \ \text{ for } \ s \ge M \big\}.$$

Moreover, let $\Omega_3(t)$ denote the cubic B-spline function given by

$$\Omega_3(t) = \begin{cases} \dfrac{1}{2}|t|^3 - t^2 + \dfrac{2}{3}, & |t| \le 1, \\ -\dfrac{1}{6}|t|^3 + t^2 - 2|t| + \dfrac{4}{3}, & 1 < |t| < 2, \\ 0, & |t| \ge 2. \end{cases}$$

It is easily checked that $\Omega_3(t)$ is twice continuously differentiable with compact support in $[-2, 2]$. Therefore, for f_κ^{app} and $\theta_f \in B_c$, we can approximately express them as the linear combinations of cubic B-spline functions

$$f_\kappa^{app}(t) = \sum_{j=0}^{N_1} a_j h_j(t), \quad \theta_f(t) = \sum_{j=0}^{N_1} a_j^\theta h_j(t) \tag{4.3}$$

in numerical experiments, where $N_1 \in \mathbb{N}$ and $h_j(t)$ is defined by

$$h_j(t) = \begin{cases} 1, & j = 0, \\ \Omega_3\left(\dfrac{t - w_j}{q}\right), & \text{otherwise} \end{cases}$$

for a fixed constant $q > 0$ and N_1 different constant w_j. In numerical examples, w_j are assumed to be N_1 points equally distributed on $[-cut, cut]$ for a fixed constant $cut > 0$.

Following [32], we represent ∂D in polar coordinates by

$$g_\kappa^{app}(t) = \rho_g(t)[\cos t, \sin t]^\top, \quad \theta_g(t) = \rho_g^\theta(t)[\cos t, \sin t]^\top, \quad 0 \leqslant t \leqslant 2\pi, \tag{4.4}$$

where

$$\rho_g(t) = \frac{b_0}{\sqrt{2\pi}} - \sum_{j=1}^{N_2}\left(\frac{b_j}{j^2}\frac{\cos jt}{\sqrt{\pi}} + \frac{b_{j+N_2}}{j^2}\frac{\sin jt}{\sqrt{\pi}}\right),$$

$$\rho_g^\theta(t) = \frac{b_0}{\sqrt{2\pi}} - \sum_{j=1}^{N_2}\left(\frac{b_j^\theta}{j^2}\frac{\cos jt}{\sqrt{\pi}} + \frac{b_{j+N_2}^\theta}{j^2}\frac{\sin jt}{\sqrt{\pi}}\right),$$

and we note

$$\boldsymbol{m}_j(t)=\begin{cases}\dfrac{1}{\sqrt{2\pi}}[\cos t,\sin t]^\top, & j=0,\\ -\dfrac{\cos jt}{j^2\sqrt{\pi}}[\cos t,\sin t]^\top, & j=1,\dots,N_2,\\ -\dfrac{\sin(j-N_2)t}{(j-N_2)^2\sqrt{\pi}}[\cos t,\sin t]^\top, & j=N_2+1,\dots,2N_2.\end{cases}$$

Furthermore, the exact scattered field u_κ^s is taken at the points $x_i\in\Gamma_{mea}, i=1,2,\dots,N_3$, which distribute equidistantly on the line segment Γ_{mea}. If we define the column vectors

$$\begin{aligned}&\boldsymbol{a}_\kappa=[a_{0,\kappa},a_{1,\kappa},\dots,a_{N_1,\kappa}]^\top, \qquad \boldsymbol{a}_\kappa^\theta=\left[a_{0,\kappa}^\theta,a_{1,\kappa}^\theta,\dots,a_{N_1,\kappa}^\theta\right]^\top,\\ &\boldsymbol{b}_\kappa=[b_{0,\kappa},b_{1,\kappa},\dots,b_{2N_2+1,\kappa}]^\top, \quad \boldsymbol{b}_\kappa^\theta=\left[b_{0,\kappa}^\theta,b_{1,\kappa}^\theta,\dots,b_{2N_2+1,\kappa}^\theta\right]^\top.\end{aligned}$$

Then the linearized equation (4.2) is reduced to the following finite-dimensional linear system:

$$\begin{bmatrix}\boldsymbol{J}_{\kappa,f} & \boldsymbol{J}_{\kappa,g}\end{bmatrix}\begin{bmatrix}\boldsymbol{a}_\kappa^\theta\\ \boldsymbol{b}_\kappa^\theta\end{bmatrix}=\boldsymbol{r}_\kappa, \tag{4.5}$$

where

$$\boldsymbol{J}_{\kappa,f}:=\left[\mathcal{F}'_{\kappa,f}[f^{app},g^{app};h_j](x_i)\right]_{N_3\times N_1}, \quad \boldsymbol{J}_{\kappa,g}:=\left[\mathcal{F}'_{\kappa,g}[f^{app},g^{app};\boldsymbol{m}_j](x_i)\right]_{N_3\times(2N_2+1)},$$

and $\boldsymbol{r}_\kappa=[r_1,r_2,\dots,r_{N_3}]^\top$ with $r_i:=u_\kappa(x_i)-\mathcal{F}_\kappa[f^{app},g^{app}](x_i)$. For convenience, we rewrite (4.5) as

$$\boldsymbol{J}_\kappa\boldsymbol{\Delta}_\kappa^\theta=\boldsymbol{r}_\kappa, \tag{4.6}$$

where

$$\boldsymbol{J}_\kappa=\begin{bmatrix}\boldsymbol{J}_{\kappa,f} & \boldsymbol{J}_{\kappa,g}\end{bmatrix}, \quad \boldsymbol{\Delta}^\theta=\left[\boldsymbol{a}_\kappa^\theta;\boldsymbol{b}_\kappa^\theta\right].$$

Notice that $\mathcal{F}'_\kappa:=[\mathcal{F}'_{\kappa,f},\mathcal{F}'_{\kappa,g}]$ is the compact operator of $C_0^2(\mathbb{R})\times C^2([0,2\pi],\mathbb{R}^2)$ into $L^2(\Gamma_{mea})$, which leads to that the system (4.6) is ill-posed. So we will turn to solving the following regularization system:

$$(\alpha\boldsymbol{I}+\boldsymbol{J}_\kappa^*\boldsymbol{J}_\kappa)\boldsymbol{\Delta}_\kappa^\theta=\boldsymbol{J}_\kappa^*\boldsymbol{r}, \tag{4.7}$$

where $\alpha>0$ is a regularization parameter. Since $\boldsymbol{J}_\kappa$ is a complex matrix and $\boldsymbol{r}_\kappa$ is a complex vector, we use $[\mathrm{Re}(\boldsymbol{J}_\kappa);\mathrm{Im}(\boldsymbol{J}_\kappa)]$ and $[\mathrm{Re}(\boldsymbol{r}_\kappa);\mathrm{Im}(\boldsymbol{r}_\kappa)]$ instead of $\boldsymbol{J}_\kappa$ and $\boldsymbol{r}_\kappa$, respectively, to obtain a real vector $\boldsymbol{\Delta}_\kappa^\theta$.

Next, we introduce the relative error $\varepsilon(\kappa,f_\kappa^{app},g_\kappa^{app})$ by

$$\varepsilon\big(\kappa,f_\kappa^{app},g_\kappa^{app}\big):=\frac{\left\|u^s_{\kappa,f_\kappa^{app},g_\kappa^{app}}(x)-u_\kappa^s(x)\right\|_{L^2(\Gamma_{mea})}}{\left\|u_\kappa^s(x)\right\|_{L^2(\Gamma_{mea})}}$$

with the reconstructed rough surface f_κ^{app} and the reconstructed embedded obstacles g_κ^{app} and the wavemumber $\kappa>0$, where $u_\kappa^s(x)$ is the measurement data corresponding to the exact rough surface Γ and the exact obstacles D, and $u^s_{\kappa,f^{app},g^{app}}(x)$ is the scattered field with the reconstructed rough surface $\Gamma_{f^{app}}$ and the reconstructed obstacles $D_{g^{app}}$. Given the wavenumber $\kappa>0$, the tolerance $\varepsilon_\kappa\in(0,1)$ and the measurement data $u_\kappa^s|_{a,b}$, the inversion algorithm can be given as Algorithm 4.1.

Based on the Algorithm 4.1, an approximate reconstruction f_κ^{app} and g_κ^{app} can be obtained numerically for the rough surface Γ and obstacles D with a fixed wavenumber $\kappa > 0$ and the relative error $\varepsilon(\kappa, f_\kappa^{app}, g_\kappa^{app})$. Next, we will propose an iterative algorithm with multi-frequency scattered field data in order to get a more accurate reconstruction for Γ and D. Assume that the measurements $u_\kappa^s|_{\Gamma_{mea}}$ are available for the wavenumber $\kappa = \kappa_j$ with $j = 1, 2, \ldots, M$. Given the tolerance $\varepsilon_0 \in (0, 1)$, the initial guess f_0^{app} and g_0^{app}, finally, and a fixed constant $\rho \in (0, 1)$, the inversion algorithm is summarized as in Algorithm 4.2.

Algorithm 4.1: Simultaneous Reconstruction of the Locally Rough Surface Γ and the Obstacles D by Newton-type Iterative Methods for a Fixed Wavenumber κ.

1 Choose an initial guess $f_{0,\kappa}^{app}$ in the form of (4.3) for Γ with the coefficient vector $\boldsymbol{a}_{0,\kappa}$ and an initial guess $g_{0,\kappa}^{app}$ in the form of (4.4) for D with the coefficient vector $\boldsymbol{b}_{0,\kappa}$.

2 Calculate the scattered field $u^s_{\kappa, f_{m-1,\kappa}, g_{m-1,\kappa}}$ on Γ_{mea}, provided the $(m-1)$-step approximation $f_{m-1,\kappa}^{app}$ $(m \geq 1)$ and $g_{m-1,\kappa}^{app}$ $(m \geq 1)$ is known with the coefficient $\boldsymbol{a}_{m-1,\kappa}$ and $\boldsymbol{b}_{m-1,\kappa}$.

3 Solve $\boldsymbol{\Delta}_{m,\kappa}$ of Eq. (4.7) to obtain an update $f_{m,\kappa}^{app}$ with the coefficient $\boldsymbol{a}_{m,\kappa} = \boldsymbol{a}_{m-1,\kappa} + \boldsymbol{a}_{m,\kappa}^{\theta}$ and an update $g_{m,\kappa}^{app}$ with the coefficient $\boldsymbol{b}_{m,\kappa} = \boldsymbol{b}_{m-1,\kappa} + \boldsymbol{b}_{m,\kappa}^{\theta}$. Finally, calculate the relative error $\varepsilon(\kappa, f_{m,\kappa}^{app}, g_{m,\kappa}^{app})$. If

$$\left|\varepsilon\big(\kappa, f_{m,\kappa}^{app}, g_{m,\kappa}^{app}\big) - \varepsilon\big(\kappa, f_{m-1,\kappa}^{app}, g_{m-1,\kappa}^{app}\big)\right| < \varepsilon_\kappa,$$

the iteration stops; otherwise go to step 2.

Algorithm 4.2: Simultaneous Reconstruction of the Locally Rough Surface Γ and the Obstacles D by Newton-type Iterative Methods with Multifrequency Scattered Data.

1 Set $f_{0,\kappa_1}^{app} := f_0^{app}$ and $g_{0,\kappa_1}^{app} := g_0^{app}$ and $\varepsilon_{\kappa_1} := \varepsilon_0$ when $j = 1$. Otherwise, set $f_{0,\kappa_j}^{app} := f_{\kappa_{j-1}}^{app}$ and $g_{0,\kappa_j}^{app} := g_{\kappa_{j-1}}^{app}$ and $\varepsilon_{\kappa_j} := \rho\varepsilon(\kappa_{j-1}, f_{\kappa_{j-1}}^{app}, g_{\kappa_{j-1}}^{app})$ for $j \geq 2$.

2 For each $j \geq 1$, obtain an approximation $f_{\kappa_j}^{app}$ for the rough surface Γ and an approximation $g_{\kappa_j}^{app}$ for the obstacles D with the corresponding relative error $\varepsilon(\kappa_j, f_{\kappa_j}^{app}, g_{\kappa_j}^{app})$ by the Algorithm 4.1. Then, set $j := j + 1$. If $j \leq M$, go to step 1; otherwise, the iteration stops.

5. Numerical Results

This section is devoted to the numerical results of the inverse problem with both the exact and noisy data. Without loss of generality, all numerical examples are generated by Algorithm 4.2 and the multi-frequency wavenumbers are taken as $\kappa_1 = (1, 2), \kappa_2 = (3, 4), \kappa_3 = (5, 6)$ and $\kappa_4 = (7, 8)$, respectively. In numerical experiments we use the Morozov discrepancy principle to choose the regularization factor α. The noise data $u^s_{\delta,\kappa_j}(x)$ is given by

$$u^s_{\delta,\kappa_j}(x) = u^s_{\kappa_j}(x) + \delta\frac{\lambda}{\|\lambda\|}\left\|u^s_{\kappa_j}\right\|_{L^2(\Gamma_{mea})},$$

where $\lambda = \lambda_1 + i\lambda_2$ with $\lambda_1, \lambda_2 \in N(0, 1)$. Here, $N(0, 1)$ is the normal distribution with Expectation 0 and Variance 1.

5.1. The case of none embedded obstacles

In this subsection, we just present the numerical reconstructions of locally rough interfaces by Algorithm 4.2. The scattered field is measured on a line $\Gamma_{mea} := [-20, 20] \times 8$ in the upper half-space. We set $N_1 = 30, N_3 = 20, q = 1, cut = 15, \varepsilon_0 = 0.01$ and $\rho = 0.5$ in all numerical examples in this subsection.

Example 5.1. In the first example, the locally rough interface Γ is described as

$$f(t) = 0.9 \exp(-0.5t^2), \tag{5.1}$$

where the local perturbation totally lies above the planar interface Γ_0. Figs. 5.1-5.2 show the reconstructions from the exact data and 10% noisy data, respectively.

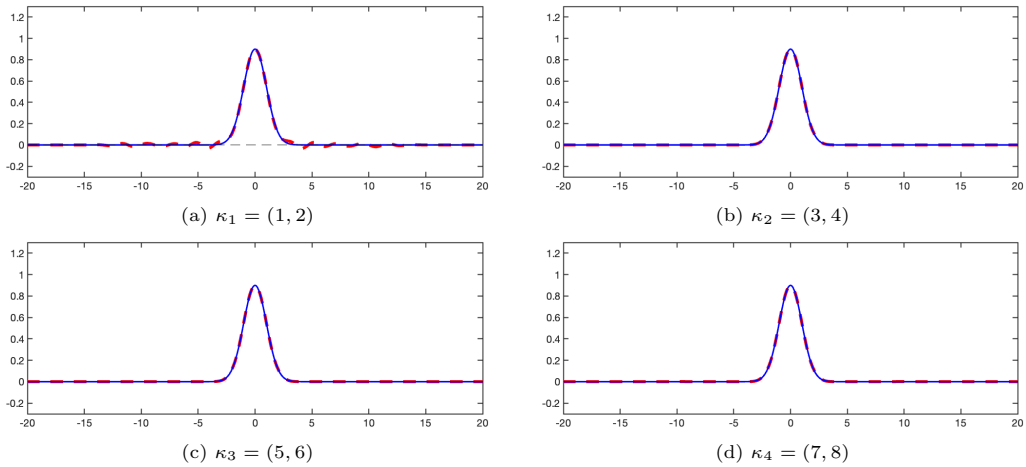

(a) $\kappa_1 = (1, 2)$ (b) $\kappa_2 = (3, 4)$

(c) $\kappa_3 = (5, 6)$ (d) $\kappa_4 = (7, 8)$

Fig. 5.1. Comparison of the reconstructed interface (red dashed line) with the real interface (blue solid line) for exact data and the black dashed line in (a) represents the initial value of the iteration.

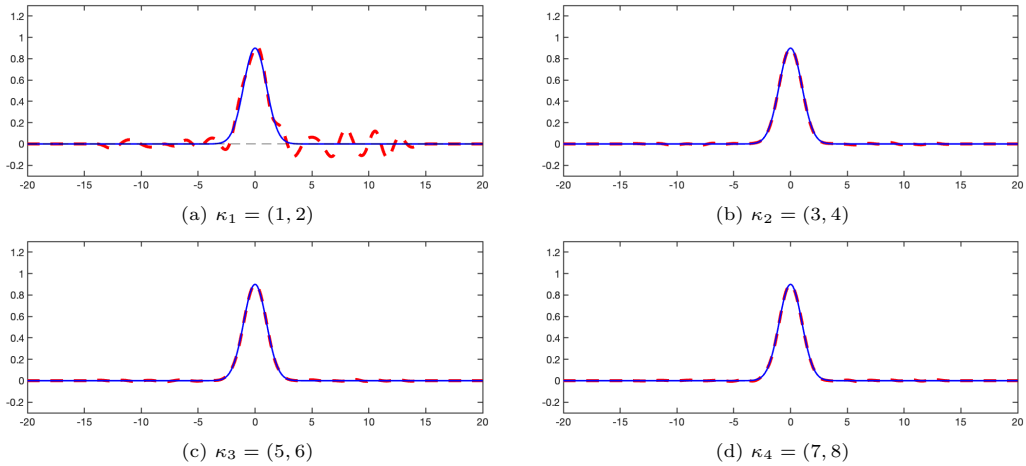

(a) $\kappa_1 = (1, 2)$ (b) $\kappa_2 = (3, 4)$

(c) $\kappa_3 = (5, 6)$ (d) $\kappa_4 = (7, 8)$

Fig. 5.2. Comparison of the reconstructed interface (red dashed line) with the real interface (blue solid line) for 10% noise data and the black dashed line in (a) represents the initial value of the iteration.

Example 5.2. In the second example, we try to reconstruct a more complex interface which is described as

$$f(t) = 0.9\cos(0.5\pi t)\exp(-0.05t^2) + 0.6\sin(0.5\pi t)\exp\big(-0.05(t-3)^2\big) - 0.6\sin(0.25\pi t)\exp\big(-0.05(t+5)^2\big). \tag{5.2}$$

Figs. 5.3-5.4 show the reconstructions from the exact data and 10% noisy data, respectively.

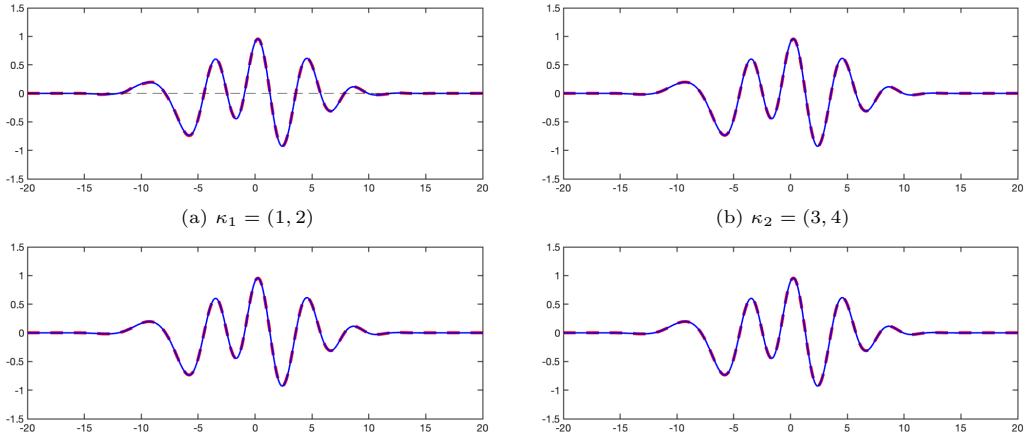

(a) $\kappa_1 = (1, 2)$ (b) $\kappa_2 = (3, 4)$

(c) $\kappa_3 = (5, 6)$ (d) $\kappa_4 = (7, 8)$

Fig. 5.3. Comparison of the reconstructed interface (red dashed line) with the real interface (blue solid line) for exact data and the black dashed line in (a) represents the initial value of the iteration.

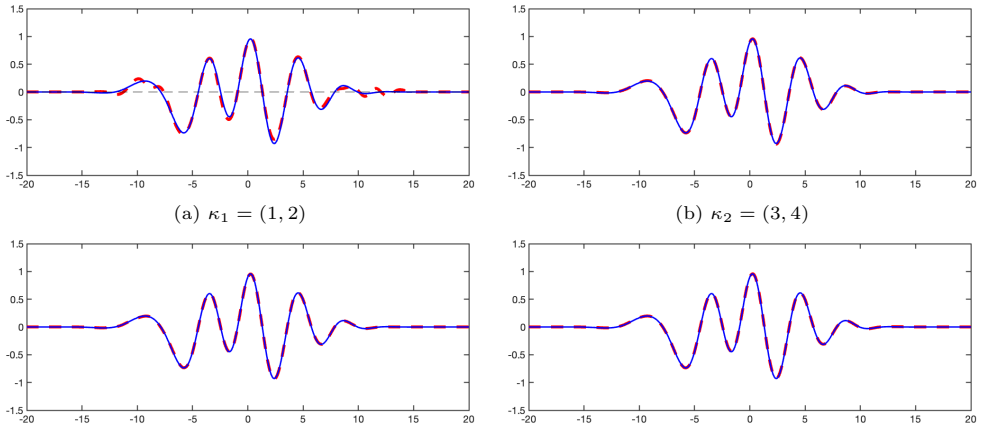

(a) $\kappa_1 = (1, 2)$ (b) $\kappa_2 = (3, 4)$

(c) $\kappa_3 = (5, 6)$ (d) $\kappa_4 = (7, 8)$

Fig. 5.4. Comparison of the reconstructed interface (red dashed line) with the real interface (blue solid line) for 10% noise data and the black dashed line in (a) represents the initial value of the iteration.

Example 5.3. In the third example, we try to consider the multiscale profile interface, which is defined as

$$f(x_1) = \begin{cases} 4\exp\big(1/\big((t/16)^2-1\big)\big)\big(0.5+0.05\sin\big(16\pi(t/20)\big)\big), & x_1 \in [-15, 15], \\ 0, & \text{elsewhere.} \end{cases} \tag{5.3}$$

Figs. 5.5-5.6 show the reconstructions from the exact data and 10% noisy data, respectively.

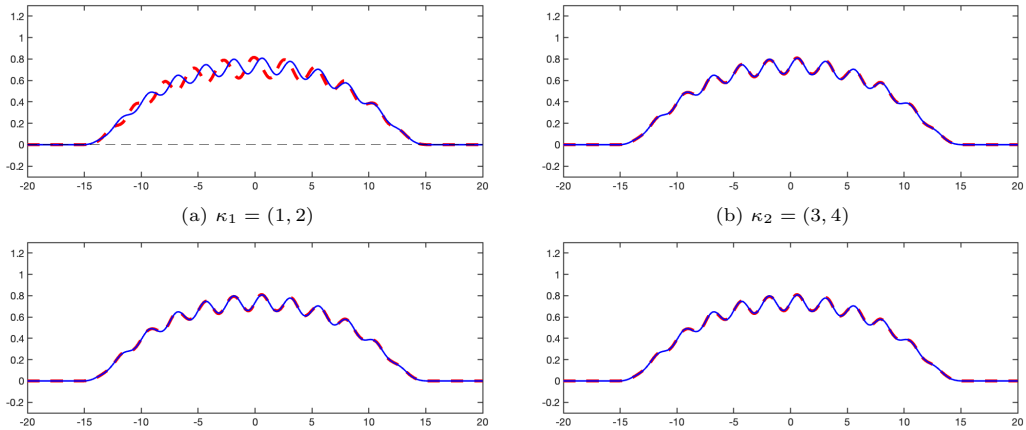

(a) $\kappa_1 = (1, 2)$ (b) $\kappa_2 = (3, 4)$

(c) $\kappa_3 = (5, 6)$ (d) $\kappa_4 = (7, 8)$

Fig. 5.5. Comparison of the reconstructed interface (red dashed line) with the real interface (blue solid line) for exact data and the black dashed line in (a) represents the initial value of the iteration.

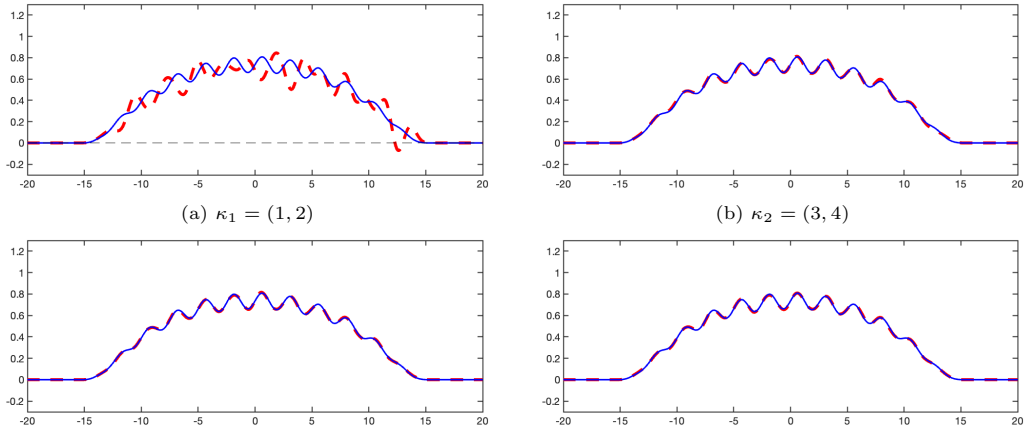

(a) $\kappa_1 = (1, 2)$ (b) $\kappa_2 = (3, 4)$

(c) $\kappa_3 = (5, 6)$ (d) $\kappa_4 = (7, 8)$

Fig. 5.6. Comparison of the reconstructed interface (red dashed line) with the real interface (blue solid line) for 10% noise data and the black dashed line in (a) represents the initial value of the iteration.

5.2. The case of embedded obstacles

In this subsection, we use Algorithm 4.2 to reconstruct both locally rough surfaces and impenetrable sound-soft obstacles. In order to obtain a more precise reconstruction of embedded obstacles, we use $\Gamma_{mea} := [-50, 50] \times 8, N_1 = 30, N_2 = 10, N_3 = 50, q = 1, cut = 15, \varepsilon_0 = 0.01$ and $\rho = 0.5$.

Example 5.4. In the fourth example, the locally rough interface is given in (5.1) and the embedded obstacle is described as

$$x(\theta) = \big(0.6\big(2 + 0.3\cos(3\theta)\big)\cos(\theta), -8 + 0.6\big(2 + 0.3\cos(3\theta)\big)\sin(\theta)\big), \quad \theta \in [0, 2\pi).$$

Figs. 5.7-5.8 show the reconstructions from the exact data and 10% noisy data, respectively.

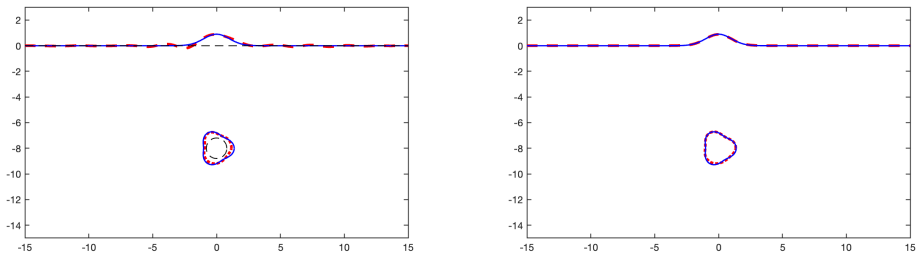

(a) $\kappa_1 = (1, 2)$ (b) $\kappa_2 = (3, 4)$

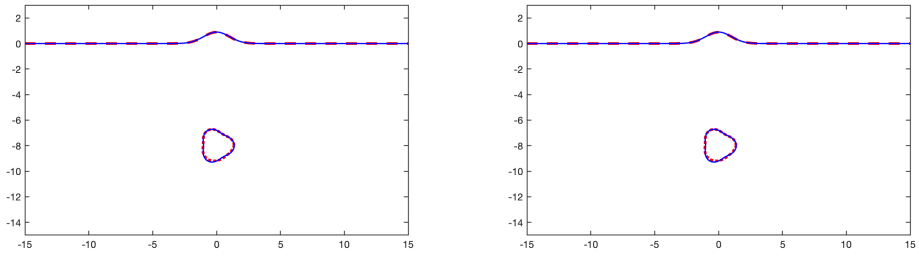

(c) $\kappa_3 = (5, 6)$ (d) $\kappa_4 = (7, 8)$

Fig. 5.7. Comparison of the reconstructed interface and obstacle (red dashed line) with the real interface and obstacle (blue solid line) for exact data and the black dashed line in (a) represents the initial value of the iteration.

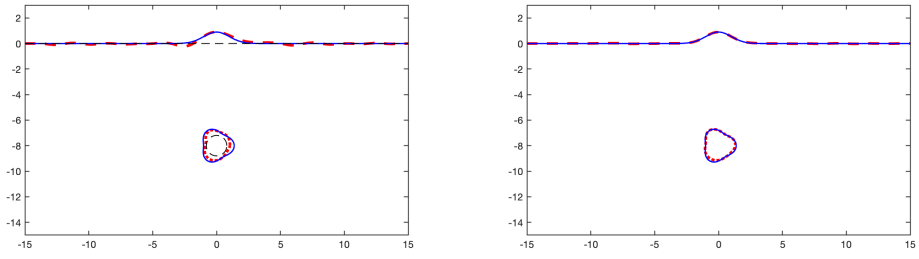

(a) $\kappa_1 = (1, 2)$ (b) $\kappa_2 = (3, 4)$

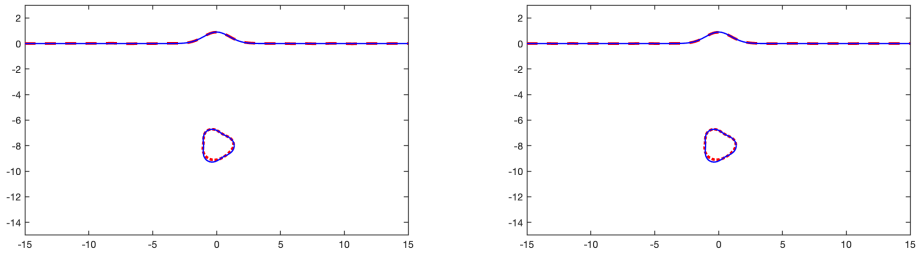

(c) $\kappa_3 = (5, 6)$ (d) $\kappa_4 = (7, 8)$

Fig. 5.8. Comparison of the reconstructed interface and obstacle (red dashed line) with the real interface and obstacle (blue solid line) for 10% noise data and the black dashed line in (a) represents the initial value of the iteration.

Example 5.5. In the fifth example, the locally rough interface is given in (5.2) and embedded obstacles is described as

$$x(\theta) = \big(-5 + 0.6\big(\cos^3(\theta) + \cos(\theta)\big), -8 + 0.6\big(\sin^3(\theta) + \sin(\theta)\big)\big), \quad \theta \in [0, 2\pi).$$

Figs. 5.9-5.10 show the reconstructions from the exact data and 10% noisy data, respectively.

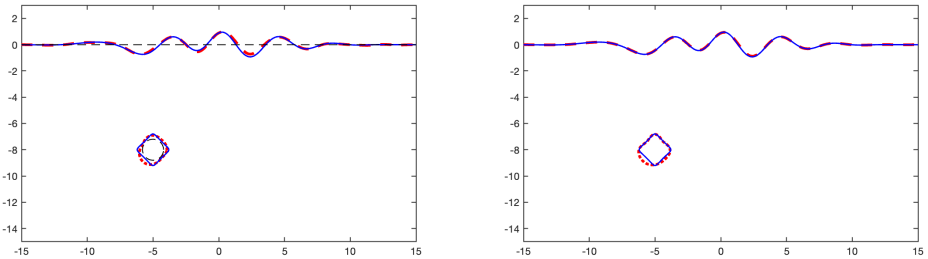

(a) $\kappa_1 = (1, 2)$ (b) $\kappa_2 = (3, 4)$

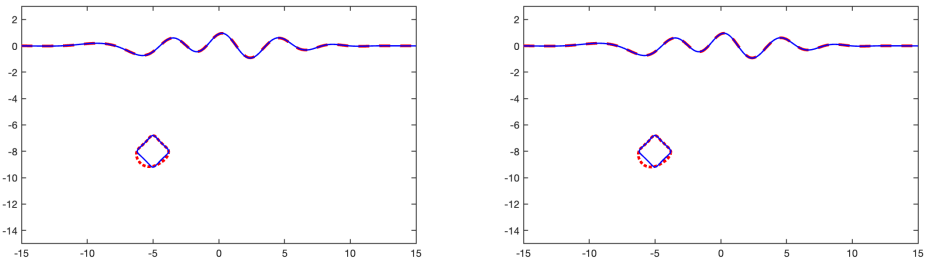

(c) $\kappa_3 = (5, 6)$ (d) $\kappa_4 = (7, 8)$

Fig. 5.9. Comparison of the reconstructed interface and obstacle (red dashed line) with the real interface and obstacle (blue solid line) for exact data and the black dashed line in (a) represents the initial value of the iteration.

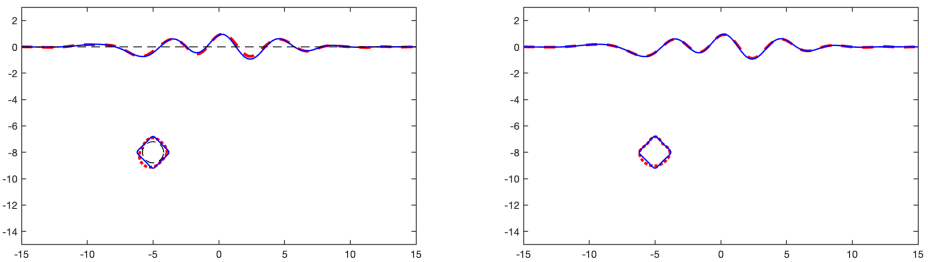

(a) $\kappa_1 = (1, 2)$ (b) $\kappa_2 = (3, 4)$

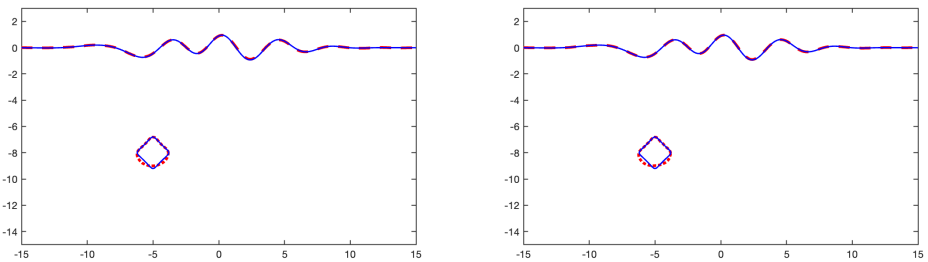

(c) $\kappa_3 = (5, 6)$ (d) $\kappa_4 = (7, 8)$

Fig. 5.10. Comparison of the reconstructed interface and obstacle (red dashed line) with the real interface and obstacle (blue solid line) for 10% noise data and the black dashed line in (a) represents the initial value of the iteration.

The above numerical results illustrate that the Newton iteration algorithm with multi-frequency data gives a stable and accurate reconstruction for a wide variety of the locally rough surfaces and embedded obstacles even in the presence of 10% noise in measurements. Moreover, it is also seen from Examples 5.4 and 5.5 that the numerical reconstruction is more better for

the interface than the buried obstacles. This is because the measurements are just taken in the upper half-space.

6. Conclusion

In this paper, we proposed a Newton-type iterative algorithm for the simultaneous reconstruction of locally rough interfaces and embedded obstacles via multi-frequency near-field measurements, where a complete differentiability analysis was established by introducing one kind of shape derivatives and reducing the original problem into an integral system in the bounded domain. Numerical results show that the inversion algorithm can provide stable and accurate reconstruction to capture the different geometrical features of infinite interface and embedded obstacles. Furthermore, along with the lines, the inversion algorithm could also be extended to solve inverse electromagnetic scattering problems associated with an infinite rough interface. We hope to report on these works in the future.

Acknowledgements. This work was supported by the National Key R&D Program of China (Project No. 2021YFF050 1501) and by the NNSF of China (Grant No. 12326607).

References

[1] H. Ammari, E. Iakovleva, and D. Lesselier, A MUSIC algorithm for locating small inclusions buried in a half-space from the scattering amplitude at a fixed frequency, *SIAM Multiscale Model. Simul.*, **3** (2005), 597–628.

[2] G. Bao, G. Hu, and T. Yin, Time-harmonic acoustic scattering from locally perturbed half-planes, *SIAM J. Appl. Math.*, **78** (2018), 2672–2691.

[3] G. Bao and P. Li, Near-field imaging of infinite rough surfaces, *SIAM J. Appl. Math.*, **73** (2013), 2162–2187.

[4] G. Bao and P. Li, Near-field imaging of infinite rough surfaces in dielectric media, *SIAM J. Imaging Sci.*, **7** (2014), 867–899.

[5] G. Bao and J. Lin, Imaging of local surface displacement on an infinite ground plane: The multiple frequency case, *SIAM J. Appl. Math.*, **71** (2011), 1733–1752.

[6] C. Burkard and R. Potthast, A multi-section approach for rough surface reconstruction via the Kirsch-Kress scheme, *Inverse Problems*, **26** (2010), 045007.

[7] S.N. Chandler-Wilde, P. Monk, and M. Thomas, The mathematics of scattering by unbounded, rough, inhomogeneous layers, *J. Comput. Appl. Math.*, **204** (2007), 549–559.

[8] S.N. Chandler-Wilde and R. Potthast, The domain derivative in rough-surface scattering and rigorous estimates for first-order perturbation theory, *Proc. R. Soc. Lond.*, **A458** (2002), 2967–3001.

[9] S.N. Chandler-Wilde and B. Zhang, On the solvability of a class of second kind integral equations on unbounded domains, *J. Math. Anal. Appl.*, **214** (1997), 482–502.

[10] S.N. Chandler-Wilde and B. Zhang, Scattering of electromagnetic waves by rough interfaces and inhomogeneous layers, *SIAM J. Math. Anal.*, **30** (1999), 559–583.

[11] L. Chorfi and P. Gaitan, Reconstruction of the interface between two-layered media using far-field measurements, *Inverse Problems*, **27** (2011), 075001.

[12] D. Colton and R. Kress, *Inverse Acoustic and Electromagnetic Scattering Theory*, Springer, 2019.

[13] M. Ding, J. Li, K. Liu, and J. Yang, Imaging of locally rough surfaces by the linear sampling method with the near-field data, *SIAM J. Imaging Sci.*, **10** (2017), 1579–1602.

[14] B. Gebauer, M. Hanke, A. Kirsch, W. Muniz, and C. Schneider, A sampling method for detecting buried objects using electromagnetic scattering, *Inverse Problems*, **21** (2005), 2035–2050.

[15] R. Griesmaier, An asymptotic factorization method for inverse electromagnetic scattering in layered media, *SIAM J. Appl. Math.*, **68** (2008), 1378–1403.
[16] A. Henrot and M. Pierre, *Shape Variation and Optimization. A Geometric Analysis*, EMS Tracts Math., 2018.
[17] F. Hettlich, Fréchet derivatives in inverse obstacles scattering, *Inverse Problems*, **11** (1995), 371–382.
[18] F. Hettlich, Fréchet derivatives in inverse obstacles scattering, *Inverse Problems*, **14** (1998), 209–210.
[19] T. Hohage, *Iterative Methods in Inverse Obstacles Scattering: Regularization Theory of Linear and Nonlinear Exponentially Ill-posed Problems*, PhD Thesis, University of Linz, 1999.
[20] A. Kirsch, The domain derivative and two applications in inverse scattering theory, *Inverse Problems*, **9** (1993), 81–96.
[21] R. Kress and L. Päivärinta, On the far field in obstacles scattering, *SIAM J. Appl. Math.*, **59** (1999), 1413–1426.
[22] R. Kress and T. Tran, Inverse scattering for a locally perturbed half-plane, *Inverse Problems*, **16** (2000), 1541–1559.
[23] A. Lechleiter, *Factorization Methods for Photonics and Rough Surfaces*, PhD Thesis, Karlsruher Institut für Technologie, 2008.
[24] J. Li, P. Li, H. Liu, and X. Liu, Recovering multiscale buried anomalies in a two-layered medium, *Inverse Problems*, **31** (2015), 105006.
[25] J. Li, G. Sun, and R. Zhang, The numerical solution of scattering by infinite rough interfaces based on the integral equation method, *Comput. Math. Appl.*, **71** (2016), 1491–1502.
[26] J. Li, G. Sun, and B. Zhang, The Kirsch-Kress method for inverse scattering by infinite locally rough interfaces, *Appl. Anal.*, **96** (2017), 85–107.
[27] J. Li, J. Yang, and B. Zhang, A linear sampling method for inverse acoustic scattering by a locally rough interface, *Inverse Probl. Imaging*, **15** (2021), 1247–1267.
[28] J. Li, J. Yang, and B. Zhang, Near-field imaging of a locally rough interface and buried obstacles with the linear sampling method, *J. Comput. Phys.*, **464** (2022), 1247–1267.
[29] L. Li, J. Yang, B. Zhang, and H. Zhang, Imaging of buried obstacles in a two-layered medium with phaseless far-field data, *Inverse Problems*, **37** (2021), 055004.
[30] L. Li, J. Yang, B. Zhang, and H. Zhang, Direct imaging methods for reconstructing a locally rough interface from phaseless total-field data or phased far-field data, *SIAM J. Imaging Sci.*, **17** (2024), 188–224.
[31] L. Li, J. Yang, B. Zhang, and H. Zhang, Uniform far-field asymptotics of the two-layered green function in two dimensions and application to wave scattering in a two-layered medium, *SIAM J. Math. Anal.*, **56** (2024), 4143–4184.
[32] Z. Li, Z. Deng, and J. Sun, Extended-sampling-Bayesian method for limited aperture inverse scattering problems, *SIAM J. Imaging Sci.*, **13** (2020), 422–444.
[33] C. Lines, *Inverse Scattering by Unbounded Rough Surfaces*, PhD Thesis, Brunel University, 2003.
[34] C. Lines and S.N. Chandler-Wilde, A time domain point source method for inverse scattering by rough surfaces, *Computing*, **75** (2005), 157–180.
[35] M. Liu and J. Yang, Numerical reconstruction of locally rough surfaces with a Newton iterative algorithm, *Commun. Comput. Phys.*, **33** (2023), 884–911.
[36] X. Liu, B. Zhang, and H. Zhang, A direct imaging method for inverse scattering by unbounded rough surfaces, *SIAM J. Imaging Sci.*, **11** (2018), 1629–1650.
[37] L. Mönch, A Newton method for solving the inverse scattering problem for a sound-hard obstacles, *Inverse Problems*, **12** (1996), 309–323.
[38] D. Natroshvili, T. Arens, and S.N. Chandler-Wilde, Uniqueness, existence, and integral equation formulations for interface scattering problems, *Mem. Differential Equations Math. Phys.*, **30** (2003), 105–146.

[39] R. Potthast, Fréchet differentiability of the solution to the acoustic Neumann scattering problem with respect to the domain, *J. Inv. Ill-Posed Problems*, **4** (1996), 67–84.

[40] R. Potthast, Domain derivatives in electromagnetic scattering, *Math. Methods Appl. Sci.*, **19** (1996), 1157–1175.

[41] F. Qu, B. Zhang, and H. Zhang, A novel integral equation for scattering by locally rough surfaces and application to the inverse problem: The Neumann case, *SIAM J. Sci. Comput.*, **41** (2019), A3673–A3702.

[42] D.G. Roy and S. Mudaliar, Domain derivatives in dielectric rough surface scattering, *IEEE Trans. Antennas Propag.*, **63** (2015), 4486–4495.

[43] M. Thomas, *Analysis of Rough Surface Scattering Problems*, PhD Thesis, The University of Reading, 2006.

[44] X. Xu, B. Zhang, and H. Zhang, Uniqueness and direct imaging method for inverse scattering by locally rough surfaces with phaseless near-field data, *SIAM J. Imaging Sci.*, **12** (2019), 119–152.

[45] J. Yang, J. Li, and B. Zhang, Simultaneous recovery of a locally rough interface and the embedded obstacles with its surrounding medium, *Inverse Problems*, **38** (2022), 045011.

[46] H. Zhang, Recovering unbounded rough surfaces with a direct imaging method, *Acta Math. Appl. Sin. Engl. Ser.*, **36** (2020), 119–133.

[47] H. Zhang and B. Zhang, A novel integral equation for scattering by locally rough surfaces and application to the inverse problem, *SIAM J. Appl. Math.*, **73** (2013), 1811–1829.